AES Clean Energy
40’ CEN Battery Energy Storage System Project
Battery Energy Storage System (BESS) Level
Fire Risk Assessment

20221215-CEN-AW0423-BESS-FRA-R0

Issued: 5 January 2023

Prepared for:

AES Clean Energy
4300 Wilson Blvd, ,
Arlington, VA 24639

Issued by:

Hiller
2120 Capital Drive
Wilmington NC 28405

Table of Contents

Revision History

Revision	Date	Description
0	5 January 2023	Issued for Client Dissemination

Executive Summary

This containerized battery energy storage system (BESS) Fire Risk Assessment (FRA) evaluates the 40' CEN BESS in a bounding design basis fire event per the requirements of NFPA 855, Section 4.1.4.2 to evaluate the fire risk associated with the thermal runaway of a single unit. While global energy storage market sector BESS does not readily demonstrate container-to-container fire propagation, this FRA establishes the maximum theoretical design basis accident heat flux that could be realized by an adjacent BESS separated by a 6.5' passageway. This FRA is intended to demonstrate the maximum theoretical heat flux for a typical installation to demonstrate how the 40'CEN BESS may perform in a design basis fire accident.

The methodologies used in this AES Clean Energy Fire Risk Assessment are based on internationally recognized Process Safety Management principles for the reliance on recognized and generally accepted good engineering practices. These engineering practices utilizes numerous international consensus standards and market sector testing data to ensure the efficacy of the quantitative analysis. Specifically, the Society of Fire Protection Engineers (SFPE) Engineering Guide, *Fire Risk Assessments* was utilized to frame the Fire Risk Assessment format to be compliant with the requirements of the National Fire Protection Association (NFPA) Standard 551, *Guide for the Evaluation of Fire Risk Assessments*. Where necessary to compute the radiant heat at the adjacent Energy Storage Units and structure adjacencies, the *SFPE Handbook of Fire Protection Engineering* and NFPA *Fire Protection Handbook* as well as other peer-reviewed research and publications were relied upon to establish the technical basis for the applicable computations. The application of each standard and peer reviewed document is referenced throughout this report.

This Fire Risk Assessment is a fundamental element that defines a bounding theoretical fire scenario to be integrated into the NFPA 855 required Hazard Mitigation Analysis. This FRA is a fundamental element of the integrated documents necessary for submittal in accordance with NFPA 855 and the International Fire Code (IFC) Section 1207.

A Fire risk assessment is a common engineering decision making tool for the estimation and evaluation of *fire risk* for credited fire scenarios and their probabilities and consequences. This Fire Risk Assessment is used to establish the documented technical basis supporting risk and engineering management decisions. The enabling scenario is an unmitigated fire where all non-certified Safety Integrity Level (SIL) components fail to operate.

While today's energy storage safety codes and standards acknowledge cascading thermal runaway as a risk, they stop short of prohibiting it, and fail to address the risk of non-flaming heat transfer to adjacent structures or equipment [1]. Therefore, to address the associated risk, the magnitude of the fire risk is quantified and presented herein.

Based on our continued research, and the completed numerical analysis, there remains approximately less than a 1% likelihood across the global battery energy storage system market sector that an event resulting in an exothermic reaction and thermal runaway could occur. In the event the theoretical bounding design basis accident scenario of a complete fire engagement of the CEN Solutions 40' Battery Energy Storage System (BESS) is realized, there is an estimated Peak Heat Release Rate of approximately 107 MW. The corresponding temperature of the compartmental gases after 3000 seconds will be approximately 1635 ^{o}K (1362 ^{o}C). Using classical heat transfer calculations the uninsulated (worst case) internal wall temperature will be 1514 ^{o}K (1241 ^{o}C). The external wall temperature due to heat lost to the surrounding environment will

be approximately 1514 °K (1241°C). The centerline temperature of the plume will be approximately 926 °K (629 °C). The total radiant heat flux, considering geometric focus factors, from the radiated heat emanating from the fully engage container (754 kW/m^2) and released fire plume (1.2 kW/m^2) will be approximately 755.6 kW/m^2.

Assuming a design basis wind of 4.16 m/s, the calculated surface temperature of a first responder at a distance of 6.5 feet (3.048 m) passageway could intermittently reach as high as 1383 K (1110 °C).

While very unlikely based on the global ESS market sector of cascading fires between adjacent containerized battery energy storage systems, if a design basis fire event is realized and is unnoticed and unmitigated, the an adjacent 4-‘ CEN BESS Thermal Management System should be able to control the internal environment but could eventually shutdown when internal temperatures exceed pre-established setpoints (typically 90°F/32 °C). Once the internal thermal management is no longer in operation, the heat transfer from the adjacent fully developed container fire could, as a function of the fire lifecycle and thermal insulation degradation, will could exceed the thermal stability thresholds of the adjacent racks.

It is recommended that additional mitigation measures (evaporative cooling) be considered within the required Hazard Mitigation Analysis to control adjacent BESS surface temperatures to lessen the probability of cascading container fire propagation.

Scope

This product level Fire Risk Assessment (FRA) identifies and quantifies the potential fire and heat flux hazards associated with AES Clean Energy 40' Battery Energy Storage Container Energy Storage Project (BESS) within the 40' CEN BESS. The 40' CEN BESS utilizes the Samsung SDI 112 Ah E4L NMC battery technology [2-5]. This product level FRA is based on an assumed installation adjacent within Sun City Arizona to characterize the performance of the BESS.

No adjacencies were evaluated as project level design documentation was not provided. This FRA is based on a theoretical installation. A final FRA will be required for actual installations that considers all the project level and environmental variables.

The results of this FRA are intended to establish the technical basis for fire risk management decisions.

This Fire Risk Assessment was conducted in accordance with the requirements and guidelines of the:

- NFPA 551, *Guide for the Evaluation of Fire Risk Assessments* [6]
- SFPE G.04:2006 – *Engineering Guide: Fire Risk Assessment*; [7]
- NFPA No.: HFPE-01 - SFPE Handbook of Fire Protection Engineering [8]
- ISO 16732-1: 2012 – Fire Safety Engineering – Fire Risk Assessment, Part 1: General[9]
- ISO 16732-3: 2012 – Fire Safety Engineering – Fire Risk Assessment, Part 3: Example of an Industrial Property [10]

This FRA is intended to be used to support engineering decisions when estimating the likelihood of an asset fire and to address the questions of:

(1) Identifying potentially important accident scenarios ("what can go wrong"),
(2) Determining their consequences ("what can happen when something goes wrong"), and
(3) Assessing their likelihood ("how likely is it that something will go wrong")

Purpose and Objectives

The use of Lithium-ion (Li-ion) battery-based energy storage systems (ESS) has grown significantly over the past few years. In the United States alone, Li-ion battery (LIB) use has gone from 1 MW to almost 700 MW in the last decade (refer to Figure 2) [11]. Many of these systems are smaller installations located in commercial occupancies, such as office buildings or manufacturing facilities. Yet, there has been relatively little research conducted on large commercial or industrial systems that can be used to ensure that effective fire protection strategies are in place.

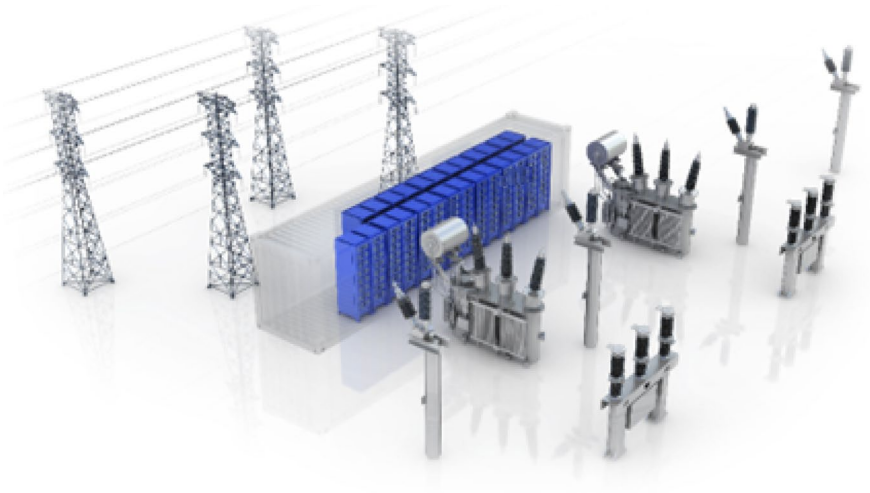

Figure 1: AES Clean Energy Utility-Energy Storage Concept

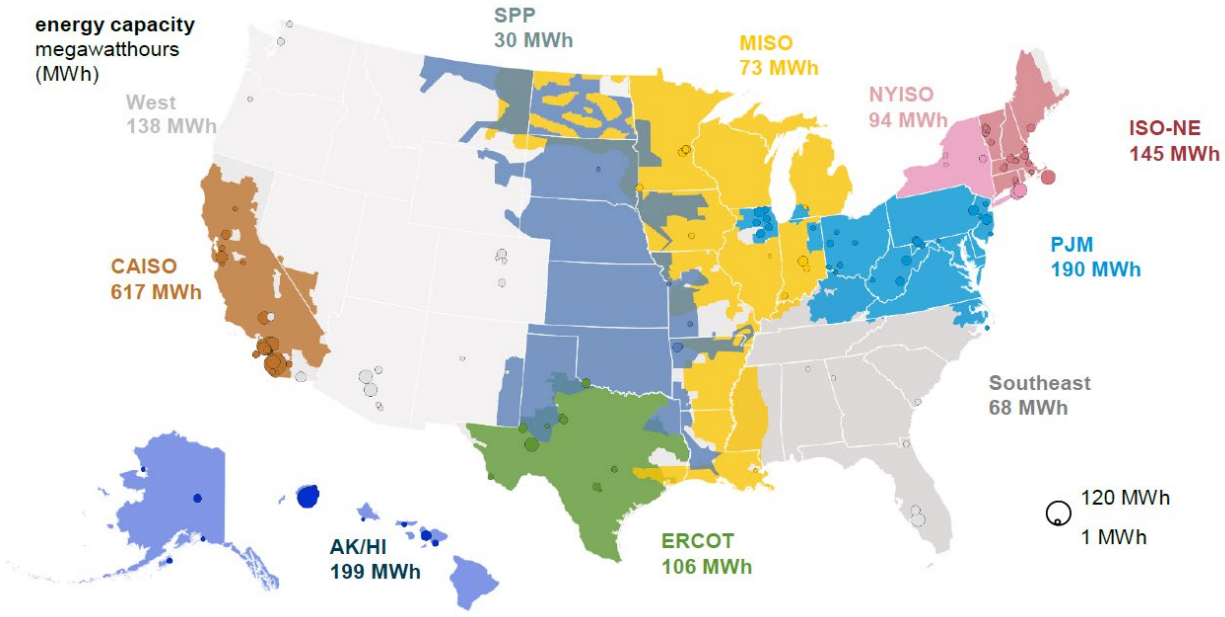

Figure 2: US Large Scale Battery Storage Installations by Region (2021)[11]

Many studies have addressed how failure of a single cell battery is affected by characteristics such as chemistry, electrolyte composition, state-of-charge (SOC), or format [12-22]. The subsequent propagation of thermal runaway to adjacent cells in a multiple cell battery module have also be studied and characterized.

From a fire protection and fire risk perspective, the overall fire hazard of any ESS is a combination of all the combustible system components, including battery chemistry, battery form factors (e.g., cylindrical, prismatic, polymer pouch), battery capacity and energy density, state of change (SoC), materials of construction, and component design (e.g., battery, module). To ensure confidence in the resulting fire protection guidance, the ESS was assumed to be operating under normal electrical operation where

electrical abuse may occur, such that any proprietary electronic protection systems, e.g., battery management system (BMS), were limited in mitigative response. Any benefit from these proprietary systems would further reduce the overall hazard, (e.g., the likelihood of ignition), but is not necessary or sufficient to ensure the adequacy of the fire protection or response measures [23, 24].

The Samsung SDI UL9540A Module Level Test demonstrated cell-to-cell propagation with ignition of the flammable gases[3]. While the 40' CEN Solutions BESS includes the Samsung SDI Thermal Management System that directly injects Novec 1230 into a module experiencing thermal runaway, the direct injection system has not been certified to be compliant with ASME B31.3 as required by UL9540, the system is not assumed to be operational to establish the bounding design basis fire event.

As part of this Fire Risk Assessment, the body of knowledge was researched, collected, reviewed, and summarized related to LIB ESSs to establish the technical basis for performance and any potential mitigation measures. The sources used includes the Department of Energy (DOE) Safety Roadmap, relevant international consensus codes and standards, incident reports, related test plans, peer-reviewed research, and previous fire testing/research with the objective of identifying the inherent risks associated with the deployment of the LIB ESS technology to life (occupants or fire fighters) and for property (asset) protection.

Continuity of Operations is specifically excluded from this assessment as no administrative controls are assumed to limit the resultant hazard.

The literature review conducted as part of this Assessment is intended to identify potential knowledge or technology gaps in the information currently available.

Assessment Methodology

This Fire Risk Assessment and the format of this report employs both qualitative and quantitative methods to determine the inherent risks of the lithium-ion battery (LIB) energy storage system (ESS) technology and follows the guidance outlined in the SFPE Engineering Guide to *Application of Risk Assessment in Fire Protection Design* and the National Fire Protection Association (NFPA) Standard 551 *Guide for the Evaluation of Fire Risk Assessments* [6, 7].

The *SFPE Guide to Fire Risk Assessments* recommends the use of risk assessment methodologies in the design and assessment of building and/or process fire safety. This guide is a recognized and generally accepted and good engineering approach to fire risk assessments. The SFPE guide provides direction to practitioners in the selection and use of fire risk assessment methodologies used to determine adequacy of design for fire safety. It also provides guidance to project stakeholders in addressing fire risk acceptability. Furthermore, the SFPE guide establishes recommended processes to be considered for the use of risk assessment methodologies and provides references to available detailed sources of information on risk assessment methodologies, procedures, and data sources. However, the SFPE Guide to Fire Risk Assessments does not provide specific fire risk assessment methodologies or tools; nor does this guide provide specific data or acceptance criteria for use in the risk assessment process. Therefore, in the absence of specific quantification methodologies, the *SFPE Handbook of Fire Protection Engineering* [8] and the *Fire Protection Handbook* [25] as well as other peer-reviewed publications were used to identify the characteristic equations for calculating compartmental fires, heat release rates (HRRs), flammable gas temperatures, and surface temperatures.

The following figure outlines the process outlined in the SFPE Guide. The format of this report closely follows

the recommendations of the SFPE Fire Risk Assessment Guide.

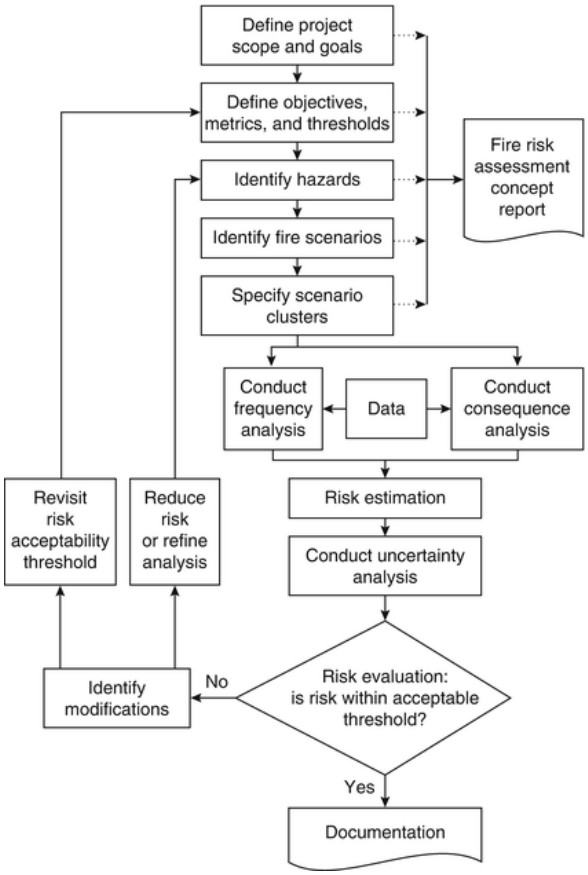

Figure 3: SFPE Fire Risk Assessment Process Flow Chart

Definition of the Project Scope

This BESS Level FRA was developed in support of the AES Clean Energy to characterize the fire performance of the 40' CEN BESS installed in a theoretical installation. As a conservative measure, due to the environmental considerations (elevation, humidity, wind directions and velocities) the theoretical installation is located in in Sun City Arizona.

This project focuses on the inherent fire hazards and risks associated with the Samsung SDI lithium-ion battery (LIB) technology and limits the fire generated from the flammable gas emitted from one-Stack Level and determines the potential impacts to the surrounding adjacent structures [26]. This steady-state FRA leverages the qualitative information gained through an exhaustive literature review of the failure rates (the total number of failures within an item population, divided by the total time expended by that population, during a particular measurement interval under stated conditions) and consequences of LIB within the global ESS market sector, as well as calculates the heat flux generated from a fully engaged stack fire within a given ESS. In the absence of specific failure data of a manufacturer's part number, comparable and approximate reliability data presented in the Electronic Parts Reliability Database (EPRD), Non-electrical Parts Reliability Database (NPRD) or Failure Modes/Mechanisms Database (FMD).

Analysis Enabling Assumptions

The following enabling assumptions were used to facilitate this Fire Risk Assessment to characterize a worst case scenario:

- Designed engineering controls for BMS or supplemental controls are assumed to be operable, but in a degraded condition to mitigate exothermic reaction.
- Ambient conditions are assumed to be standard pressure temperature (STP).
- External environmental air conditions assume a design basis wind velocity of 1.5 m/s. Ambient temperature is 295 ^{o}K (22 ^{o}C/72 ^{o}F).
- UL 9540A testing of the comparable Modules Level Test for the Samsung SDI E4L Unit, and the associated measured temperatures are the best available data of heat release rates and associated target wall temperatures are assumed to be representative of containerized/compartmentalized BESS gas layer temperatures.
- Numerical/analytical methodologies employed are based on SFPE,NFPA Handbooks, or other peer-reviewed publications and are assumed to be adequate for characterizing the critical calculation variables, and are cited herein.

Construction of the Samsung SDI NMC Battery Cell

This BESS Level Fire Risk Assessment uses the best available information to characterize the associated risks with the LIB technologies. The Samsung SDI BESS design has an integrated solution containing the Samsung SDI Power Battery Cell, Model Number CS1120RT001A, 3.63VDC, 112Ah technology as shown in Table 1.

Table 1: SAMSUNG E4L Cell Under Test

Cell	
Manufacturer	Samsung SDI
Model Number	CS1120RT001A
Chemistry	NMC (Lithium Nickel Manganese Cobalt Oxide (LiNiMnCoO2))
Nominal Electrical Ratings	3.63VDC, 112Ah
Dimensions	174*46.2*133mm
Weight	2100 g
Construction Description	Prismatic, Cell with UL approval
Tested to UL 1642	Yes
Tested to UL 1973	Yes
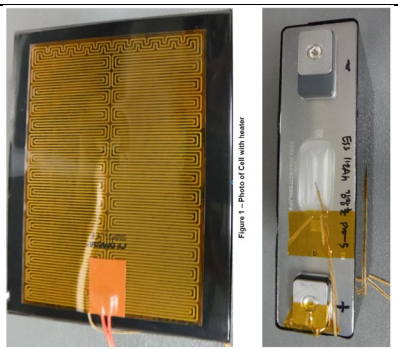	

As it pertains to the design and construction of the Samsung SDI battery modules, research of the failure modes and mechanisms of NMC cells was conducted as part of this analysis. It is assumed the published research on typical NMC failure mechanisms are comparable to the Samsung SDI Model CS1120RT001A cells. Therefore, the following discussion is based on comparable NMC battery chemistry and form factors to establish a technical basis upon which failure mechanics and performance characteristics could be extrapolated to support this analysis.

Figure 4: Samsung SDI MS1304E101A Module

Lithium-ion batteries have many advantages but the reactive, volatile and flammable materials present in the battery are a concern and may be a threat to auto-induced thermal runaway temperature and voltage [14]. Although not demonstrated within the BESS market sector by the Samsung SDI MS1304E101A battery modules, as shown in the UL9540A tests overheating may start exothermal reactions that release even more heat which in turn can lead to an accelerated thermal runaway and propagation between cells [2-5]. Research and industry experience indicates thermal runaway could be initiated due to overcharge, over-discharge, mechanical deformation, external heating or an external or internal short circuit. The heat generated by any of these events may start exothermal reactions in the battery that in turn could lead to cell venting, fire or explosion [20, 27-30]. These risks are well known and are not only associated with the heat and high temperatures that may develop, the emission of harmful or poisonous gases also pose a danger that has been emphasized in literature but also other gases which can be flammable may be emitted. The reactions during overheating are typically due to the decomposition of the solid electrolyte interphase (SEI) layer, anode and cathode as well as electrolyte decomposition and combustion.

In general, when Li-ion battery failure is induced by thermal or electrical abuse, the failure eventually evolves into a thermal runaway [31]. The failures may be induced by external forces (i.e., severe mechanical shock or damage or internal/external thermal transients leading to damage), internal shorting (i.e., manufacturing induced defects, dendrite formation, metal particles, poison), or the poor thermal stability of Li-ion cells during uncontrolled overcharging or discharging [31]. Research has shown that when a number of lithium-ion cells are used in a battery pack, there is always a disproportional *capacity distribution band* due to the individual battery state of charge, thermal performance, and “variation of capacity” between different cells [32]. This capacity band will continue to broaden throughout the battery pack as a function of the number of charging cycles, and eventually, the capacity of a battery pack will be limited by the cell with the lowest capacity . Thus, the lowest capacity cell may experience overcharge and over-discharge through the charging/discharging

cycles. This has been proven to be the case, even if the whole pack is experiencing normal charge/discharge cycles, inducing electrical abuse and potentially leading to thermal runaway. Without a battery management system, the capacity band of a cylindrical lithium-ion battery cannot be eliminated.

Although not specific to the Samsung SDI E4L NMC cells due to the limitation of published information, research demonstrates NMC cells within a battery pack or module are shown to degrade during testing demonstrating performance during excessive abuse. Testing objectively demonstrates that when cells fail, there is the formation of irregularities and dendrites create micro-shorting pathways during overcharge cycling conditions due to degraded cell capacity in the distribution band. Simultaneous formation of dendrites within the anode during charging eventually creates an micro-shorting pathways and increase internal heating. Research indicates an increased rate of dendrite formation occurs in overcharge conditions than in the normal charging conditions [16-20, 30].

Research of NMC Cells indicates that as temperature increases above 60 ^{o}C, the Li-ion deintercalates from anode and the solid electrolyte interface film (SEI) layer of the lithium intercalated carbon anode undergoes an exothermic decomposition reaction. As the temperature continues to increase to about 105 ^{o}C, the SEI layer further decomposes where the cathode material generally loses its protection thereby exposing the electrolyte. Sustained exposures to temperatures above 100^{o}C facilitates system breakdown resulting in the initiation of exothermic reactions between the cathode active material and electrolyte resulting in rapidly increasing temperatures.

As the temperature increases, the separator of the lithium-ion battery degrades and thins. As the exothermic reaction continues, at temperatures above 180^{o}C the separator (polypropylene) degrades, thus reducing the protective properties between the positive and negative electrodes of the cell. This results in the flow of short circuit currents and the cell enters into the thermal runaway. As the internal temperatures increase to the range of 180–250^{o}C, an exothermic reaction heat occurs between the lithium-ion positive electrode and the electrolyte. At sustained temperatures above 200^{o}C, the electrolyte decomposes, resulting in the release of significant heat from the exothermic reaction. Generally, thermal runaway occurs when an uncontrolled exothermic reaction occurs. The exothermic reaction exponentially increases due to a surge in environmental temperature causing a further increase in internal cell temperature, that could without mitigation result in an explosion/deflagration. It is proposed when temperatures are sustained above 200 °C, thermal runaway can occur spontaneously as a result of fire or explosion.

The state of charge (SOC) is a significant contributing variable to the onset of thermal runaway of NMC Cells. Other noted research indicates conditions where partially or fully discharged NMC cells, under adiabatic-like constant power heating similar to the UL9540A Module Level Test did not experience induced thermal runaway below 100°C. Therefore, it is reasonable to assume when the Samsung SDI E4L NMC cells are partially discharged and incipient battery failure occurs, thermal runaway is unlikely.

Lithium Ion Battery Hazards: Thermal Runaway – Causes and Results

Fire challenges associated with the bulk storage of Li-ion batteries are unique given the presence of a flammable organic electrolyte within the Li-ion battery as compared to the aqueous electrolytes typically found in other widely used battery types. As presented, when exposed to an external heat source (fire), Li-ion batteries can experience thermal runaway reactions resulting in the release of flammable organics and the potential rupture of the battery [33, 34].

The different stages and reactions contributing to the general thermal runaway process of a lithium ion cell have been examined and are well documented within the energy storage industry. When a lithium-ion cell experiences thermal runaway, the noted degradation occurs resulting in elevated cell surface temperatures causing cascading impacts that have been demonstrated to propagate to the surrounding environment and adjacent cells. Observations from previous tests have shown these effects are very similar for all cell types (cylindrical hard case, prismatic hard case, pouch cell). Depending on the battery system design, adjacent cells may likewise be thermally damaged enter thermal runaway.

It is well documented that cell component breakdown due to thermal runaway results in the production of hot flammable gases due to the chemical reactions mentioned above [15, 18, 19, 35-40]. The flammable gas generation occurs during cell decomposition resulting in increased internal pressure, leading to cell expansion, including the application of compressive force to adjacent parts in the system. Depending on the magnitude of the expansive forces the cells have been known to rupture encapsulation.

Upon rupture, the cell begins to vent and together with the produced gas and a chaotic mixture of hot and glowing particles are ejected from the cell. Expelled particles typically contain pieces of active material from the cell's anode and cathode. Temperature measurement of released gases for the Samsung SDI E4L NMC cells averages 150 ^{o}C. Analysis of the ejected gas showed high proportions of hydrogen, hydrocarbon, and carbon monoxide. Therefore, flammability and the risk of deflagration or explosion, based upon industry performance is given at a fuel concentration of approximately 9.21% at ambient temperatures[2-5].

The mentioned effects usually have their impact on the battery and its environment as a function of time. The Samsung SDI E4L cells time to thermal runaway ranges from 24:26 min to 27:15 min [4]. The heat release rate of a single cell thermally interacts with adjacent cells increasing the internal temperatures and challenges the integrity of the cell. This combination of effects creates the environment where subsequent cell failure will occur resulting in cascading degradation of the battery modules. Unmitigated, the entire module assembly will be damaged due to cell thermal runaway [3]. The cascading degradations process will exponentially accelerate and usually within several minutes, the battery housing may lose integrity due to the amount of thermal energy. During degradation, the prismatic cells swell and bulge during pressurization. To be compliant with UL 1642, all lithium=ion cells include safety vents that are designed to release the internal pressure of the cell when a specified pressure is reached [41]. Upon cell rupture, the gas accumulating inside the cell will be released and will react with atmospheric air (with fresh oxygen and moisture). The air exchange with the battery will react with the freshly plated lithium metal and electrolyte and may cause explosion and ignition.

The research associated with this FRA indicates the cell State of Charge (SoC) significantly and adversely impacts the reactivity of the cell during an external fire scenario. In particular, a fully charged battery has an increased propensity to undergo a thermal runaway reaction, increased initial fire growth rate and interestingly, decreased total energy release. This suggests that, to reduce the hazard potential in bulk storage, LIB should be well managed to avoid under/over-charging or being maintained at a reduced SOC [26].

Overcharge

There are a few ways in which overcharge can occur. The most obvious overcharge mode is charging a cell to too high of a voltage (over voltage, overcharge). For example, charging a 3.2 V rated cell above 5 V will likely lead to energetic failure. Charging at excessive currents, but not excessive voltages, can also cause an overcharge failure; in this case, localized regions of high current density within a cell will become

overcharged, while other regions within the cell will remain within appropriate voltage limits [13, 42].

Although controlled through the Battery Management System (BMS), severe overcharge failures are not uncommon[31]. Unless the BMS is designed to meet Safety Integrity Level (SIL) Ratings, there is the potential a design or manufacturing defect can cause bypassing of protection mechanisms and result in severe overcharge failures. As noted in the report for the ESS used globally, these types of failures also occur as a result of human error with systems that either lack hardwired protection (e.g., prototype systems that are being tested) or in charging schemes with manual voltage and current settings [31].

Although severe overcharge will lead to cell thermal runaway, repeated slight overcharge of a cell may not cause a failure for an extended timeframe, but can eventually result in thermal runaway [14, 18]. Industry response to this known problem prompted requirements in IEEE 1725 and IEEE 1625 for cell manufacturers to communicate specific high voltage limits appropriate for secondary protection settings specific to each cell design to pack and device designers who purchase their cells. IEEE 1625 adopted the concept of a safe charging current and charging voltage envelope relative to temperature [13, 33, 43].

External Short Circuit

High rate discharging (or charging) can cause resistive heating within cells at points of high impedance as indicated in the findings associated with the ESS fires within the market sector [12, 31]. Such internal heating could cause cells to exceed thermal stability limits. Points of high impedance could include weld points within a cell (internal tab attachment) or electrode surfaces. As cell size and capacity increases, the likelihood of internal impedance heating leading to thermal runaway also increases. Larger cells exhibit slower heat transfer to their exteriors, and they usually have higher capacities. Thus, they have the potential to convert more electrical energy to internal heat. UN and UL testing requirements provide a minimum requirement for cell external short circuit resistance: discharge through a resistance of less than 0.1 ohm in a 55°C (131°F) environment. International and domestic shipping regulations (as found in the US CFR, as well as IATA and ICAO publications) require that cells or batteries be protected from short-circuiting. Investigation of a number of thermal runaway failures that have occurred during transport has revealed that improper packaging, particularly a failure to prevent short circuits is a common cause of these incidents.

Over-Discharge

Research demonstrates over-discharging a lithium-ion cell to 0 V will not cause a thermal runaway reaction [27]. However, such over-discharge can cause internal damage to electrodes and current collectors, can lead to lithium plating if the cell is recharged (particularly, if the cell is repeatedly over-discharged), and can ultimately lead to thermal runaway [18]. Most BMS will allow the recharge of over-discharged cells, despite the potential for the negative electrode to become damaged [14]. Therefore, over-discharge does periodically cause thermal runaway of lithium-ion cells.

Forcing a cell into “reversal” (charging to a negative voltage, “forced over-discharge”) may also cause thermal runaway. UL 1973 and UN tests provide a minimum requirement for resistance to forced over-discharge for cells used in multi-cell packs [44]. These tests are designed to simulate the most likely mechanism of forced discharge, which occurs when a cell with lower capacity than its neighboring series elements is present in a multi-series battery pack that is externally short circuited. A lower capacity cell of this type can occur due to aging of the battery pack. In this scenario, current flow from the higher capacity series elements in the pack will drive the discharged series element into reversal. The UN and UL testing

does not include repeated forced discharge. Thus, if a system does not include protection electronics that will detect and disable charging of a damaged cell, it is possible a cell could be repeatedly force over-discharged and ultimately undergo a thermal runaway reaction.

Thermal Abuse

The most direct way to exceed the thermal stability limits of a lithium-ion cell is to subject it to excessive external heating. Industry testing relies upon the use of an external heat source that is applied to the exterior of target cells to induce localized reactions and to determine if the failure propagates to the entire module [3]. This literature review of the failure mechanisms of LIB indicates energetic field failures of LIB devices have been attributed to long-term operation of cells at temperatures just above the self-heating point of 70 to 90°C (158 to 194°F). Such failures require not only elevated temperature, but an adiabatic (highly insulated) environment, and extended times to reach a self-sustaining thermal runaway condition. If a ESS was exposed to long-term operation without environmental thermal management, significant damage could occur. Acute exposure of a cell to high temperatures will readily induce thermal runaway in that cell. As demonstrated in the UL9540A Module Level Test of the Samsung SDI E4L Series battery module, if an internal cell fault is sufficient to cause thermal runaway in a single cell of a multi-cell battery pack, heat transfer from the faulting cell can cause thermal runaway in neighboring cells of the battery pack[45]. Thus, the thermal runaway reaction will propagate through a battery rack if there is a performance issue with the Thermal Management System.

Propagation of cell thermal runaway has significant implications for fire suppression and fire protection. LIB in exothermic reactions self-generate oxygen to sustain the fire. A fire suppressant or low oxygen environment may extinguish flames from a battery pack, but the thermal runaway reaction will propagate if heat is not sufficiently removed from the adjacent cells[24]. Responders to fires involving lithium-ion battery packs have often described a series of re-ignition events. Typically, responders report they used a fire extinguisher on a battery pack fire, thought they had extinguished the fire, and then observed the fire re-ignite as an additional cell vented [42].

Risk Acceptability Thresholds and Failure Initiation

Since May 2019, there have over 30 documented stationary energy storage system fires within the global market sector. Research has shown there are four main causes that have been attributed to ESS failures that include:

- Insufficient Battery Protection Systems against electric shock [28, 31] .
- Inadequate management of operating environment
- Faulty Installations
- Insufficient ESS BMS and EMS System Integration [31].

Based on the number of recent recorded industry failures, energy storage system Battery Management Systems (when designed as non- SIL) do not have a proven track record of fire mitigation/prevention due to thermal or electrical abuse. Research has objectively demonstrated that once the critical sustainment point of an exothermic reaction is reached, a Battery Management System cannot stop or mitigate the cascading failures of adjacent cells within modules [14, 17, 20, 27, 29, 30, 33, 46].

The National Fire Protection Association (NFPA) has conducted a series of tests to determine preferable suppression systems for ESS [47, 48] and determined that water based automatic sprinkler systems was

chosen as a viable option for evaluating fire protection strategies for Li-ion batteries for lowering the exothermic reaction temperature. At present, there is no industry or standard that designates a fire protection suppression strategy for bulk packaged Li-ion cells, larger format Li-ion cells, or Li-ion cells contained in or packed with other equipment. NFPA 13 does not provide a specific recommendation for the protection of Li-ion cells or complete batteries, and it is not known if water is the most appropriate extinguishing medium for Li-ion batteries. There is limited real-scale data available to support a fire hazard assessment of Li-ion based ESS and there is no experimental data available to support sprinkler protection guidance[23, 24, 29].

Therefore, to determine the worst case scenario it is assumed the ESS that is experiencing a potential exothermic reaction and is suppressed results in a loss.

Identification of the Hazards

The major hazards for large-scale ESS systems can be categorized as electrical, mechanical and other hazards. Electrical hazards occur when there is a live contact between a person and an ESS system exposing the person to severe electric shocks. Mechanical hazards occur when there is a (unforeseen) physical collision between a person and an ESS system. Potential other hazards (mainly related to electric and electrochemical systems) include:

- Explosion hazards, caused by a rapid expansion of gases due to exothermic reaction and subsequent failure of LIB cells, modules, Stacks, and containers.
- Fire hazards, arising from combustible materials used in the storage system
- Thermal hazards, due to the thermal properties of a system or its components
- Thermal runaway hazard, causing propagation of increasing temperatures, pressures, and fire towards neighboring cells.
- Chemical hazards, caused by (unforeseen) contact between a person and toxic, acidic, corrosive
- Components leaking from the ESS system [49].

The risk of electrical shock at the system level should be mitigated by applying design rules regarding electrical insulation (e.g. containment), by wearing adequate personnel protective equipment and by imposing operational instructions. The risk of mechanical shock at the system level should be mitigated by applying design rules regarding containment. The risk of other hazards at the system level should be mitigated by applying design rules regarding containment.

To ensure safe handling in general, the following recommendations should be considered to prevent exposure to abusive environmental conditions:

- The ESS system or its components should not be opened or punctured, including during emergency operations
- The ESS system or its components should not be left in places of high temperature
- The ESS system or its components should not be exposed to condensation and high humidity and contact with water should be avoided
- The ESS system or its components should not be submitted to excessive electrical stress [49].

Therefore, this Fire Risk Assessment bounds the aforementioned risks with the most conservative hazard that is a direct result of thermal defects within LIB resulting in the cascading impacts of exothermic reactions resulting in thermal runaway. Assuming conservative quazi-linearity of the published failure

rates resulting in fire, the ESS may experience up to approximately 1% of failures depending on the level of electrical and thermal abuse [12, 32]. However, while there is no readily identifiable industry research on failure of large-scale NMC systems, recent UL9540A testing of the Samsung SDI cells objectively demonstrates a lower propensity of thermal runaway propagation [50].

Exothermic and Thermal Runaway Hazard Evaluation

Quantification of Heat Flux of a ESS Fire

Characterizing the fire hazards associated with the Samsung SDI containerized battery energy storage systems requires an understanding of the amount of energy released during the exothermic reaction of a lithium-ion battery (LIB) failure.

The potential cascading impacts associated with a fire in a lithium-ion battery ESS is significant based on the quantities of energy contained. Although the Samsung SDI modules are utilized in the 40' BESS systems has been certified and tested in accordance with UL 1973, the aforementioned fire safety features of the design is to prevent a catastrophic event in a lithium-ion ESS.

The quantification of the radiant heat flux within BESS presents several challenges due to the unavailability of proprietary information. When available, specific manufacturer data was applied. In absence of specific data, the "best available" information was used with an integrated standards-based approach with recognized and generally accepted good engineering practice. The conservative approach to radiant heat flux quantification is used to present a bounding scenario. Understandably, proximity and adjacencies of siting and spacing of ESS containers contributes a significant role in fire safety. Therefore, a radiation heat transfer analysis was used to assess separation distances between adjacent ESS containers.

The overall approach to the radiation heat transfer analysis of an ESS container fire on an exposed ESS container is based on the cited works of the *SPFE Handbook of Fire Protection Engineering* for compartmental fires [8] and those of Quintiere's works in *Fundamentals of Fire Phenomena* [51] to calculate the following:

1. Effective Heat Release Rate (HRR)
2. Mass Flow Rate within the emitting (on fire) BESS
3. Quantification of Peak Heat Release Rate of ESS Fire Event
4. Temperature of the Hot Gas Layer over time
5. Wall Temperature of the BESS Fire Source
6. Heat Transfer Coefficient
7. Smoke Plume Centerline Temperature
8. View Factors
9. Radiant and Convective Heat Flux
10. Convective and Radiative Heat Flux at the Fence Line

1. Effective Heat Release Rate (HRR)

The energy release rate (heat release rate, HRR) of the compartmental fire is based on UL 9540A testing and assumes sustained peak based on the UL9540A Cell level test data and is extrapolated to numerically characterize a worst-case scenario.

The heat release rate is the recognized single most important variable in a fire hazard[8]. The heat release

rate of a burning item is measured in kilowatts (kW). It is the rate at which the combustion reactions produce heat. The relationship of these two quantities can be expressed as

$$HRR = \Delta h_c * MLR$$

Where Δh_c is the effective heat of combustion and MLR is the Mass Loss Rate of the LIB. The mass loss rate (burning rate) of the battery is an essential element in quantifying the heat release rate; however, in comparison to the volumetric flow rates within the compartment, the mass loss rate plays a somewhat insignificant role in the total heat release rate.

Therefore, the mass flow rate of air and the heat of combustion of lithium-ion batteries combusting in air is used to approximate the peak heat release rate. A prismatic LIB has an average mass of the Samsung SDI E3L is 2.1 kg [4] . NMC Cells have an energy density of 90 to 250 W/kg [52, 53]. A mass loss rate (MLR) of 0.0015 kg/s is assumed [14].

The effective heat of combustion (Δhc) for a LIB is the heat of combustion which would be expected in a fire where incomplete combustion takes place. The effective heat of combustion is often also described as a fraction of the theoretical heat of combustion [2]. The effective heat of combustion assumed for this analysis is based on the *Thermal runaway and safety of large lithium-ion battery systems* and the Underwriters Laboratory UL 9540A testing of the Samsung SDI cells. The range of values used for this analysis is based on the interpolated data presented in the UL 9540A Cell Level Test for the Samsung SDI 112 Ah NMC cells and is assumed to be 24.2 kJ/kg for the fully engaged Stack as well as the upper range of identified effective heat of combustion [2-5, 42].

2. Mass Flow Rate within the emitting (on fire) BESS

Compartment fires with forced ventilation can significantly impact the fire growth, temperature within the compartment, spread of gases from the fire, and the decent of the smoke layer within the compartment [8]. This Fire Risk Assessment assumes normal HVAC operation throughout the event to establish a bounding scenario. It is generally understood the HVAC control will be established by the Fire Alarm Control Panel (FACP) at some interval based on internal temperature and will be de-energized. However, to establish the maximum design basis fire event, the non-SIL certified HVAC control system is assumed to fail to respond to shutdown commands and remain energized.

This scenario applies the analyzes a compartmental fire under natural convection thermal management conditions, the growth of the fire will be significantly impacted by the volumetric air flow rate within the ESS container by providing an adequate oxygen supply for the large quantity of fuel. However, it also serves as a limiting factor for the peak heat release rate of a fire in a compartment with uniform air flow.

Therefore, a compartment fire with forced-ventilation is assumed and behaves significantly different than a naturally ventilated space. A forced ventilation compartment may have an unstable gas layer due to the mixing of the combustion products and the air flow which spreads the hot gases throughout the compartment [8]. A compartmentalized forced ventilation scenario also limits the formation of the smoke layer. As in any compartment fire, the depth of the smoke layer increases over time. However, the smoke layer in forced ventilation scenarios descends until it reaches equilibrium; this phenomenon allows for additional fuel to be consumed. Once the fire reaches its peak heat release rate, the fire growth is limited

to the ventilation rate throughout the compartment. Since the ventilation rate is constant, the amount of fuel that can be consumed per second becomes constant, allowing the fire to reach a steady-state condition until all fuel within the container is consumed [8].

The mass flow of the burning fuel is given as the ratio of the fire energy release rate and the effective heat of combustion and is quantified by

$$m' = \frac{Q'}{\Delta h_c} + m'_{air}$$

Where,
Q' is the fire energy release rate
Δh_c is the effective heat of combustion
m'_{air} is the mass flow of the forced ventilation

3. Quantification of Peak Heat Release Rate of ESS Fire Event

The heat release rate (HRR) of a fully involved ESS fire is the factor that quantifies the fire source within an ESS. The HRR is defined as "the rate at which energy is generated by the burning of a fuel and oxygen mixture. As the heat release rate increases, the heat, smoke production and pressure within the area will increase and spread along available flow paths toward low pressure areas" [51]. The peak heat release rate quantifies the heat released for complete combustion of the fuel – peak burning rate [8, 25]. The most common method of quantifying the heat release rate is through Oxygen Consumption Calorimetry (OC), which assumes that the HRR is proportional to the oxygen consumed during the combustion of common organic fuels [42]. However, quantifying the heat release rate through OC methods is challenging for lithium-ion batteries due to their ability to release oxygen during failure. LIB's produce sufficient oxygen during the exothermic reaction to sustain a flame [8, 25, 51].

The heat release rate of a LIB ESS fire is interdependent on the initiating event, status of the LIB charging/discharging the quantity of fuel, environmental conditions, and the status of the ventilation conditions [13, 42, 47, 48]. To bound the conditions for determining the peak heat release rate, is assumed to be limited to the forced-ventilation air flow within the compartment [8]. Industry research on the failure mechanics of thermal runaway in large lithium-ion battery systems, the effective heat of combustion of a lithium-ion battery in air was determined to be approximately 28 to 40 kJ/kg [14, 27, 29, 30, 33, 54]. It is well published the mass flow rate of the gas layer within the compartment is dependent on the mass loss rate of the fuel (kg/s), density of air (1.2 kg/m3) and the range of volumetric airflow rates (m^3/s).

Although, it is generally understood that it is uncommon for LIBs to reach full combustion, for the purposes of bounding a quantifiable fire risk, it is assumed the combustion efficiency for oxygen containing products can be between 90 and 100%.

Therefore, the mass flow rate of the flammable gas compartmentalized fires is dependent on the temperature dependent density of the air and the volumetric flow rate of the natural convection cooling ventilation system in addition to the mass loss rate of the fuel (rate of volatile release from LIB failure) which is mechanically combined to form the mixed flammable gas layer. It is also assumed the fire engagement is the initiating source for volatile gases. The failure of any other system, structure, or component concurrent with a LIB fire event is assumed to be beyond extremely unlikely.

Various small scale tests of various types of lithium-ion batteries have indicated that between 16% and 27% of the battery mass is lost over a time period of 40 to 60 seconds [14, 18, 20]. Since different battery formats vary in mass, a few different types of commonly used lithium-ion batteries were analyzed to obtain a range of mass loss rates for various battery types. The entire mass was lost during UL9540A Module Level Test [3]. Conservatively, 25% is assumed to be consumed during a thermal runaway (TRA) event.

As part of the quantification of the peak energy released during a LIB exothermic reaction, it has been determined the mass loss rate of the battery although important, in comparison to the volumetric flow rates within the compartment, the mass loss rate is nearly negligible. Both are quantified in this analysis for consistency. Therefore, the mass flow rate of air and the heat of combustion of lithium-ion batteries combusting in air is used to approximate the peak heat release rate where

$$\dot{Q} = \Delta H_{eff} * \dot{m}$$

Where,

$$\dot{m} = \dot{m_{air}} + \dot{m}_{LIB} = \left(\rho_{air} * \dot{V}\right) + MLR_{fuel}$$

ρ_{air} is the density of air
$\dot{V}$ is the volumetric flow rate
MLR_{fuel} is the Mass Loss Rate of the LIB

Once the peak heat release is reached, the ESS compartment assumed to be fully-developed/engaged. A normalized time 3000 seconds (50 minutes) is assumed based on LIB failure tests [14, 20, 27, 29, 33, 54-57]. At this time an exothermic reaction is determined to be steady rate and will be sustained until a large percentage of the fuel is consumed.

The components of a LIB fire and the associated release of volatile gasses and sustainment of the exothermic reaction included in the thermal breakdown of the module and battery includes the separators, packaging, and electrolyte of LIBs. The gases potentially vented during a thermal runaway reaction may include:

The following list of emitted gases are based on an independent third party Nationally Recognized Testing Laboratory (NRTL) cell, module, and unit testing in accordance with UL 9540a, *Test Method for Evaluating Thermal Runaway Fire Propagation in Battery Energy Storage Systems* [57, 58]. The volume of gas measured during the test is provided in Figure 8.

The gases vented during a thermal runaway reaction include:

- Acetylene
- Ethylene
- Methane
- Methanol
- Propane
- Formaldehyde [37, 38, 59-61]

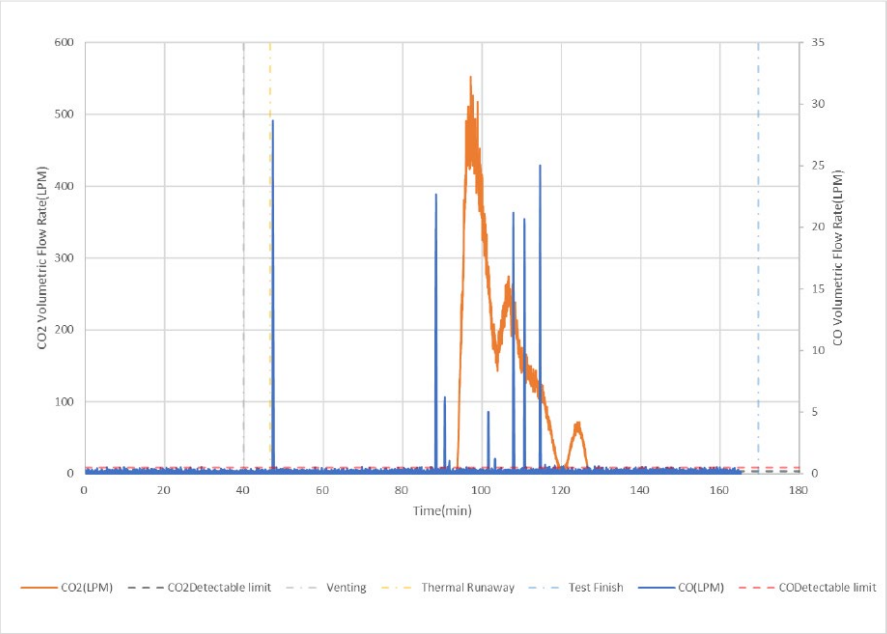

Figure 5: Results of Flammable Gas Monitoring during NRTL Testing of UL 9540A emitted from the Samsung SDI Module [3]

With the large quantity of batteries and corresponding energy stored within these systems, a large amount of fuel and flammable gases will be generated during exothermic reaction leading to a potential deflagration. For the purposes of establishing bounding conditions for this Fire Risk Assessment, it is reasonable to assume that flammable volatiles will continued to be released from failing cells even after the peak heat release rate has been reached. As the temperature continues to rise in the containerized BESS, excess unburnt fuel vapors will continue to be released contributing to the temperature increase of the gaseous mass within the container. The Samsung SDI E4L cell released 212 liters during the UL9540A Cell Level Test and 5911 liters of flammable gas during the UL9540A Module Level Test [3, 4]. The Samsung SDI MS1304E101A module result in TRA propagation between cells and fire. The Samsung SDI MS1304E101A module weight was not obtainable as the module was completely consumed as shown in Figure 6 [3].

It is recognized the Novec Direct Injection System was able to cool the thermal runaway event documented in the Samsung SDI Unit Level Test. However, the design of the Direct Injection System cannot respond and cool subsequent thermal runaway events. Therefore, while not likely subsequent TRA and module to module propagation is assumed [62-64].

.

Figure 6: Samsung SDI Module MS1304E101A UL9540A Module Level Test Result.

The resultant calculated Peak Heat Release Rate for the 40' CEN Solutions BESS is 107.2MW.

4. Temperature of the Hot Gas Layer over time

Research conducted for this FRA has identified recommendations from the *SFPE Fire Protection Engineering Handbook* [25] a suitable method for calculating the temperature rise of the upper gas layer in a compartmentalized fire is through the method of McCaffrey, Quintiere, and Harkleroad (MQH) [25]. The MQH method applies the conservation of energy principle to the hot gas layer, which gives the following

$$\frac{\Delta T_g}{T_\infty} = \frac{\frac{\dot{Q}}{\dot{m}_g c_p T_\infty}}{1 + \frac{A h_g}{\dot{m}_g c_p}}$$

Where
$\frac{\Delta T_g}{T_\infty}$ is the Change in Temperature above ambient overtime
$\dot{Q}$ is the Heat Release Rate (kW)
$\dot{m}_g$ is the Mass Flow Rate of gas layer (kg/s)
Cp is the Specific Heat of Air (kJ/kg-K)
T_∞ is the Ambient Air Temperature (^{o}K)
h_g is the Heat Transfer Coefficient (kW/m^{2}K)
A is the Surface Area of Compartment Boundaries

The MQH methodology facilitates the analyzation of the compartment temperature with respect to the energy generated by the fire, the flow rate of the gas out an opening under natural ventilation ($\dot{m}_g$), the specific heat of the air (c_p), and the heat lost from the hot gas layer to the surrounding surfaces (h_g). The MQH method identifies the compartmentalized hot gas layer temperature under naturally ventilated conditions [40]. For the purposes of this FRA, it is assumed the 40' CEN container release smoke and flames through openings around the enclosure access doors to naturally ventilate to atmosphere.

Lithium-ion batteries challenge this ventilation-limited premise as sufficient oxygen is generated through the exothermic reaction for sustainability [13, 14, 20, 47, 48, 65]. Testing has shown that lithium-ion

batteries are capable of producing sparks of flaming combustion in an inert environment along with a release of significant quantities of flammable gases. Therefore, it is assumed that a substantial amount of oxygen can release during each battery failure, as a result of the decomposition of the battery's metal oxide (cathode). It is also assumed a limited oxygen concentration within the container will not stop the progression of thermal runaway within the ESS. Recent studies of LIB failures have indicated that one the ambient temperature reaches the battery thermal stability limits (typically 180 °C) thermal runaway chain-reactions may occur more readily. Although the oxygen released from the individual batteries may not be sufficient to sustain steady combustion within a ventilation-limited compartment, masses of flammable gases from the thermal runaway reactions of LIB's will continue to be released. If the container is breached, sufficient oxygen may enter the container resulting in a deflagration of flammable gases [8, 25].

The likely scenario poses over-pressurization and explosion hazards due to the mass of unburnt fuel in a closed unventilated compartment; this presents additional hazards that are outside the scope of this report.

Therefore, based on the assumption that forced ventilation will be used to mitigate hazards posed by lithium-ion batteries during failure, a forced ventilation scenario can be used to characterize a fully developed fire within an ESS. The continuous air flow into the ESS container will allow the fire to be limited to the quantity of fuel within the compartment – representing a fully-involved ESS fire event.

The hot gas layer temperature is largely impacted by the ventilation conditions within the compartment. Therefore, with the understanding of the MQH methodology constraints, it is refined by the application of the work of Foote, Pagni, and Alvares [8]. Foote, Pagni, and Alvares conducted a series of 64 fire tests with varying forced ventilation conditions [8]. From these tests, empirical constants that represent the change in the hot gas layer temperature in forced ventilation conditions were derived. Applying the MQH method, Foote, Pagni, and Alvares added data for forced ventilation fires – now referred to as the FPA method was applied to calculate the temperature of the gas layer through

$$\frac{\Delta T_g}{T_\infty} = 0.63 \left(\frac{\dot{Q}}{\dot{m}_g c_p T_\infty} \right)^{0.72} \left(\frac{A h_g}{\dot{m}_g c_p} \right)^{-0.36}$$

The calculated temperature of the heated gas mixture is 1635 °K (1362 °C) after 3000 seconds.

5. Internal Wall Temperature of the BESS Fire Source

The approach to calculating the wall temperature follows the *SFPE Fire Protection Engineering Handbook* [25] for compartmentalized fires for the application of the Peatross and Beyler method for highly conductive materials. Peatross and Beyler refined the MQH method based on the assumption normal insulating materials will have negligible impact on the total heat released during a fully engaged fire with highly conductive walls. Therefore, Peatross and Beyler ignores insulation of the container walls. This FRA follows the precedence and recognizes the existence of insulating materials but bounds the total risk through the application of Peatross and Beyler.

Therefore, the rise of the wall temperature of the container is a function of the heat transfer between the hot gas layer and the steel panel. The temperature of the panel is a function of the heat stored within the panel with respect to the steel's material properties (density, specific heat, thickness, surface area). The rise in the wall temperature is dependent on the enthalpy flow through the wall – heat into the wall from

the developed compartment fire and the outflow of heat from the wall to the external ambient environment. The gas layer throughout a mechanically ventilated compartment is assumed to be uniform, which heats the boundary layers (walls) at a constant rate.

$$m_w^{"} c \frac{dT_w}{dt} = h_g(T_g - T_w) - h_\infty T_w$$

This analyzes the heat flow into the wall from the radiant and convective heat from the hot gas layer and the heat outflow of the convective losses from the wall to the outside. According to Quintiere's *Fundamentals of Fire Phenomena* [51], the temperature rise of the wall of the ESS fire source is calculated through the application of

$$\frac{dT_w}{dt} = \frac{1}{\rho_s c_s A_w \Delta x}\left[\varepsilon\sigma(T_g^4 + T_W^4) + h_{hot} A_W (T_g - T_w) - h_\infty A_w (T_w - T_\infty)\right]$$

Where,

$\frac{dT_w}{dt}$ is the change in wall temperature above ambient over time
ρ_s is the density of the container wall steel plate
$\boldsymbol{c_s}$ is the specific heat of steel
Δx is the thickness of the steel plate
A_w is the area of the containerized BESS exposed to the hot gas layer
ε is emissivity
σ is the Boltzman's Constant
T_g is the temperature of the gas layer
T_∞ is the ambient temperature
T_w is the temperature of the wall
h_{hot} is the heat transfer coefficient (hot)
h_∞ is the heat transfer coefficient (ambient)

The calculated internal wall temperature of the heated gas mixture is 1514 °K (1241 °C) after 3000 seconds.

6. Heat Transfer Coefficient

To quantify the convective heat transfer at the boundary layer between the hot gas layer and the compartment walls, an effective heat transfer coefficient must be calculated. A heat transfer coefficient quantifies that rate at which heat is transferred from the hot gas layer of the fire through the solid wall [66]. The heat transfer coefficient used to represent the energy exchange at the hot side of the walls was based on the following equation

$$T_{wall.ext} = \sqrt{\frac{kpc}{t}}$$

Where,
k = thermal conductivity (kW/m-K)
p = density of steel (kg/m3)
c = specific heat (kJ/kg-K)

t = time (s)

This equation represents a heat transfer coefficient that is a function of the temperature dependent thermal conductivity of the steel panel, density, and specific heat of the steel with respect to time. Under ambient conditions, the heat transfer coefficient is a stagnant value, which is used to represent the convective losses to the outside of the container. This heat transfer coefficient is a function of the thermal conductivity of the steel at ambient condition and the thickness of the steel. Understanding the thermal resistivity limitations of (assumed) Polyurethane insulation of a maximum published value of 150°C and fails above the temperature limits, it is assumed the external surface temperature is 1514 °K (1241 °C) [67].

7. Fire/Smoke Plume Centerline Temperature

A characteristic accompanying the phenomenon of a BESS fire, especially in compartments in the phase of its development, is Fire Plume. For various reasons, the subject of concern may be the determination of an incipient smoke temperature. From the point of view of the used methods and extent of details, the temperature analysis of smoke and Fire Plume may be quite variable and challenging to determine. However, publications evaluated for this Fire Risk Assessment has identified the following methodology for calculating the centerline temperature for a smoke/fire plume as follows [68, 69]:

$$\Delta T_{osa} = 0.0964 \left(\frac{T_\infty}{g\, c_p^2\, \rho_o^2} \right)^{\frac{1}{3}} Q'^{\frac{2}{3}}_k (z - z_0)^{-\frac{5}{3}}$$

Where,
ΔT_{osa} is the smoke plume centerline temperature
T_∞ is the ambient temperature
g is the gravitational constant
c_p gas specific heat capacity
ρ_o ambient air density
Q'_k heat flux shared by convection
z height above the inflammable material surface
z_o Fire Plume virtual start

Understanding the plume centerline temperature is an important characteristic that contributes thermal radiation heat transfer to the adjacent containers and to the calculation of the ground level surface temperatures. Adjacent container and surface level temperatures are a function of the Configuration/View factors.

8. Configuration/View Factors

A configuration factor is a purely geometrical relation between two surfaces, and is defined as the fraction of radiation leaving one surface which is intercepted by the other surface [8]. This factor is the variable that determines the fraction of radiation received by the target, with respect to the total radiation emitted from the source. The view factor accounts for the shape, orientation, and size of both the emitter and the target as well as the separation distance between them. Since this model accounts for the radiation coming from the heated ESS container and the externally vented flames, two view factors are calculated. Therefore, the incident radiant flux from a BESS fully engaged fire (source) to an adjacent BESS (target) separated by a given distance *x*, is given by

$$\ddot{q} = EF_{12}$$

Where E is the emissivity of the transmitting medium, and F is the no-wind view factor between the source and the Target. In this case, the view factor will be the integration of the emitting side of the target and the energy emitted from escaping hot gas. It is assumed the hot gases will escape around the doors of the source and will form a pseudo-cylindrical shape. Secondly, the side of the source that radiates the thermal energy to the adjacent BESS as indicated in Figure 9.

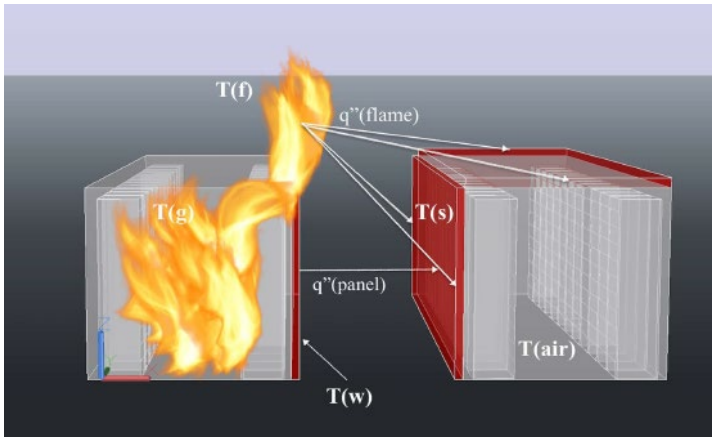

Figure 7

The view factor from the BESS radiant source to adjacent containers is a critical component of this radiation heat transfer analysis. It is within this factor that the various separation distances are accounted for. Intuitively, the radiated heat is inversely proportional to distance: a fire's intensity reduces with distance. The view factors account for the angle, separation distance, area of radiating surface/flame and the area of the target surface. The view factors for the radiating panel and cylindrical vented flames are calculated through the methods shown as follows:

Determining the geometry for the identical, parallel, directly opposing BESS containers is taken from the *SFPE Fire Protection Engineering Handbook* [25] where

$$F_{plates} = \left(\frac{2}{\pi XY}\right)\left[ln\sqrt{\frac{X_1 Y_1}{1+X^2Y^2}} + X\sqrt{1+X^2} * tan^{-1}\left(\frac{Y}{\sqrt{1+X^2}}\right) - X\tan^{-1}(X) - Y\tan^{-1}(Y)\right]$$

Where

$$X_1 = 1 + X^2$$

And

$$Y_1 = 1 + Y^2$$

X is the ratio of width to length of the BESS
Y is the ratio of height to length of the BESS

The view factor from the escaping hot gases is determined its vertical and horizontal components by

$$F_{cycl.flame.vert} = \frac{1}{\pi S} * \tan^{-1}\left(\frac{h}{\sqrt{S^2+1}}\right) - \frac{h}{\pi S} * \tan^{-1}\left(\sqrt{\frac{S-1}{S+1}}\right) + \frac{Ah}{\pi S\sqrt{A^2-1}} * \tan^{-1}\left(\sqrt{\frac{(A+1)(S-1)}{(A-1)(S+1)}}\right)$$

And

$$F_{cycl.flame.horiz} = \frac{\left(B-\frac{1}{S}\right)}{\pi\sqrt{B^2-1}} * \tan^{-1}\left(\sqrt{\frac{(B+1)(S-1)}{(A-1)(S+1)}}\right) - \frac{A-\frac{1}{S}}{\pi\sqrt{A^2-1}} * \tan^{-1}\left(\sqrt{\frac{(A+1)(S-1)}{(A-1)(S+1)}}\right)$$

Where the separation distance between the cylindrical radiant body (L), and the size of the flame (diameter (D) and flame height (H)) and,

$$S = \frac{2L}{D}$$

$$h = \frac{2H}{D}$$

$$A = \frac{h^2 + S^2 + 1}{2S}$$

$$B = \frac{1 + S^2}{2S}$$

9. Total Radiant and Convective Heat Flux

As noted, the radiant heat flux between containers is determined by the derivation of $\ddot{q} = EF_{12}$, therefore determining the total incident radiative heat flux emitted from the ESS fire source is a summation of the heat flux from the flame and the heat radiated from the steel panel. The radiant heat flux emitted by the heated panel of the ESS fire source is quantified by the correlation shown in the equation below.

$$\dot{q}_{panel.rad} = \varepsilon\sigma F_{1p,2p}(T_w^4 - T_\infty^4)$$

And

$$\dot{q}_{cyl.rad} = \varepsilon\sigma F_{1c,2c}\left(T_{fl}^4 - T_\infty^4\right)$$

Where,

ε= emissivity of surface
σ = Stefen-Boltzman Constant

$F_{1p,2p}$ = View factor from parallel BESS steel panels
$F_{1c,2c}$ = View factor from cylindrical flame exiting ESS to exposed ESS steel panel
T_w = Wall temperature of flames exiting the fire source ESS
T_{fl} = Flame temperature of flames exiting the fire source ESS
T_∞ is the ambient temperature

The calculated radiant heat flux and the external wall temperature of the fully engaged BESS is 782 kWm^2 with a surface temperature of 1514 ^oK (1241 ^oC), respectively.

10. Total Convection Heat Flux

An assumed 4.16 m/s Wind Driven Event ground level (surface) temperature due to thermal radiation heat transfer was calculated assuming the ESS container could be compromised due to the internal heat and fire during an exothermic reaction.

If there was a breach in the container integrity resulting in a release of a smoke/fire plume, the centerline temperature of the fire/smoke plume would be calculated using the following numerical analysis outlined in *SPFE Handbook of Fire Protection Engineering* for compartmental fires [2] and those of Quintiere's works in *Fundamentals of Fire Phenomena* [51]:

The centerline temperature of the fire/smoke plume was determined by:

$$\Delta T_{osa} = 0.0964 \left(\frac{T_\infty}{g\, c_p^2\, \rho_o^2} \right)^{\frac{1}{3}} Q'^{\frac{2}{3}}_k (z - z_0)^{-\frac{5}{3}}$$

Where,
ΔT_{osa} is the smoke plume centerline temperature
T_∞ is the ambient temperature
g is the gravitational constant
c_p gas specific heat capacity
ρ_o ambient air density
Q'_k heat flux shared by convection
z height above the inflammable material surface
z_o Fire Plume virtual start

Understanding the BESS acts as a radiation shield from the plume centerline point source, the magnitude of the incident thermal radiation exposure on the surface, the quantity of radiation absorbed into the ground (assumed black body) was calculated using the Mudan Method [8]as follows:

$$q'_{plume} = EF\tau$$

Where
E is the average emissive power of the plume at the flame surface
F is the view factor to the target
τ is the atmospheric transmissivity.

The thermal power of the flame is given by

$$E = E_{max}e^{-sD} + E_s[1 - e^{-sD}]$$

Where,
E_{max} is equivalent blackbody emissive power, 140 kW/m^2
s is the extinction coefficient, 0.12 m–1
D is the diameter of the fire
$E_s$is the emissive power of smoke, 20kW/m^2

The view factor of the wind driven fire/smoke plume is determined by

$$F = \sqrt{\pi {F_v}^2 + \pi {F_H}^2}$$

Where,

$$\pi F_v = \frac{a\cos\theta}{b - a\,sin\theta}\,\frac{a^2 + (b+1)^2 - 2b(1+sin\theta)}{\sqrt{AB}}\,tan^{-1}\left(\sqrt{\frac{A}{B}}\left(\frac{b-1}{b+1}\right)^{\frac{1}{2}}\right) + \frac{cos\theta}{\sqrt{C}}\,x\left[tan^{-1}\left(\frac{ab - (b^2-1)sin\theta}{\sqrt{b^2-1}\sqrt{C}}\right) + tan^{-1}\left(\frac{(b^2-1)sin\theta}{\sqrt{b^2-1}\sqrt{C}}\right)\right] - \frac{a\cos\theta}{(b - a\,sin\theta)}\,tan^{-1}\left(\sqrt{\frac{b-1}{b+1}}\right)$$

And

$$\pi F_H = tan^{-1}\left(\sqrt{\frac{b-1}{b+1}}\right) - \frac{a^2 + (b+1)^2 - 2(b+1+absin\theta)}{\sqrt{AB}}\,tan^{-1}\left(\sqrt{\frac{A}{B}}\left(\frac{b-1}{b+1}\right)^{\frac{1}{2}}\right) + \frac{sin\theta}{\sqrt{C}}\,x\left[tan^{-1}\left(\frac{ab - (b^2-1)sin\theta}{\sqrt{b^2-1}\sqrt{C}}\right) + tan^{-1}\left(\frac{(b^2-1)^{\frac{1}{2}}sin\theta}{\sqrt{C}}\right)\right]$$

Where,

a is the ratio of the Flame Height to Flame Radius (H/R)
b is the ratio of the distance between the center of the flame cylinder to the target to the flame radius
A is given by the equation $A = a^2 + (b+1)^2 - 2a(b+1)sin\theta$
B is given by the equation $B = a^2 + (b+1)^2 - 2a(b-1)sin\theta$
C is given by the equation $C = 1 + (b^2+1)cos\theta$

Atmospheric absorption

The radiation from the fire to surrounding objects will be partially attenuated by absorption and scattering along the intervening path. The principal constituents of the atmosphere that absorb thermal radiation are water vapor (H2O) and carbon dioxide (CO2) [8]. The atmospheric transmissivity is given by

$$\tau = 1 - \alpha_w - \alpha_c$$

Where the carbon dioxide vapor absorption coefficient is,

$$\alpha_c = \varepsilon_c \left(\frac{T_a}{T_s}\right)^{0.65}$$

The partial pressure of CO2 remains relatively constant at about $3x10^{-4}$ atm. The emissivity of the carbon dioxide band is shown in Figure 10 [8].

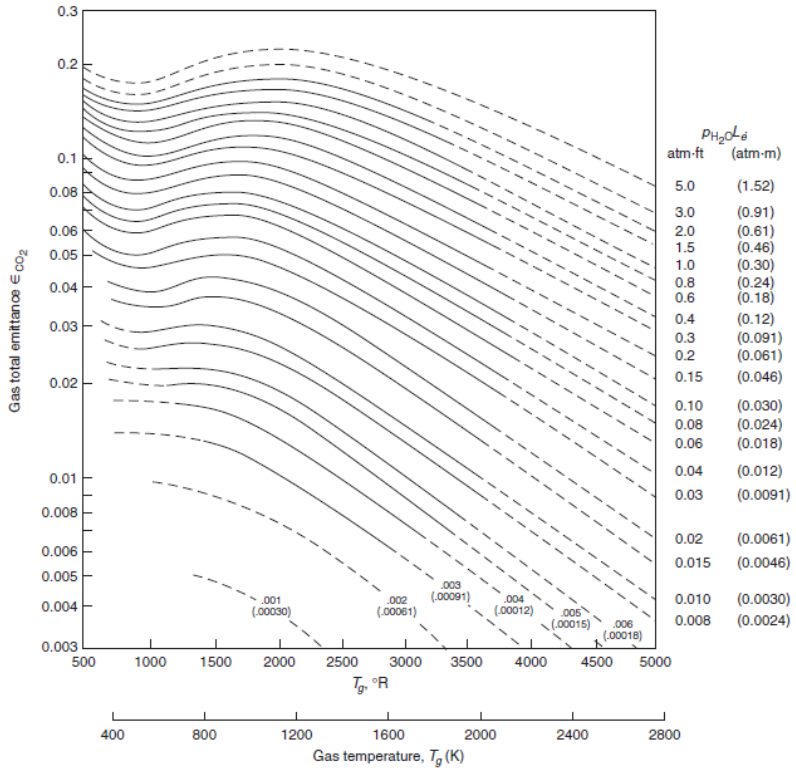

Figure 8Total emissivity of carbon dioxide in a mixture of total pressure of 1 atm [2]

And the water vapor absorption coefficient is

$$\alpha_w = \varepsilon_w \left(\frac{T_a}{T_s}\right)^{0.45}$$

Where ε_w is determined by the partial pressure of water vapor,

$$p'_w = \frac{RH}{100} e^{\left(14.4114 - \frac{5328}{T_a}\right)}$$

And the pathlength from the flame surface to the target is

$$p_w L = p'_w L \left(\frac{T_s}{T_a}\right)$$

The source temperature, and $p_w L$, determine the water vapor emissivity, ε_w, using emissivity plots given in Figure 11.

Where the centerline temperature was determined to be approximately 913°K. The atmospheric transmissivity is approximately 0.95.

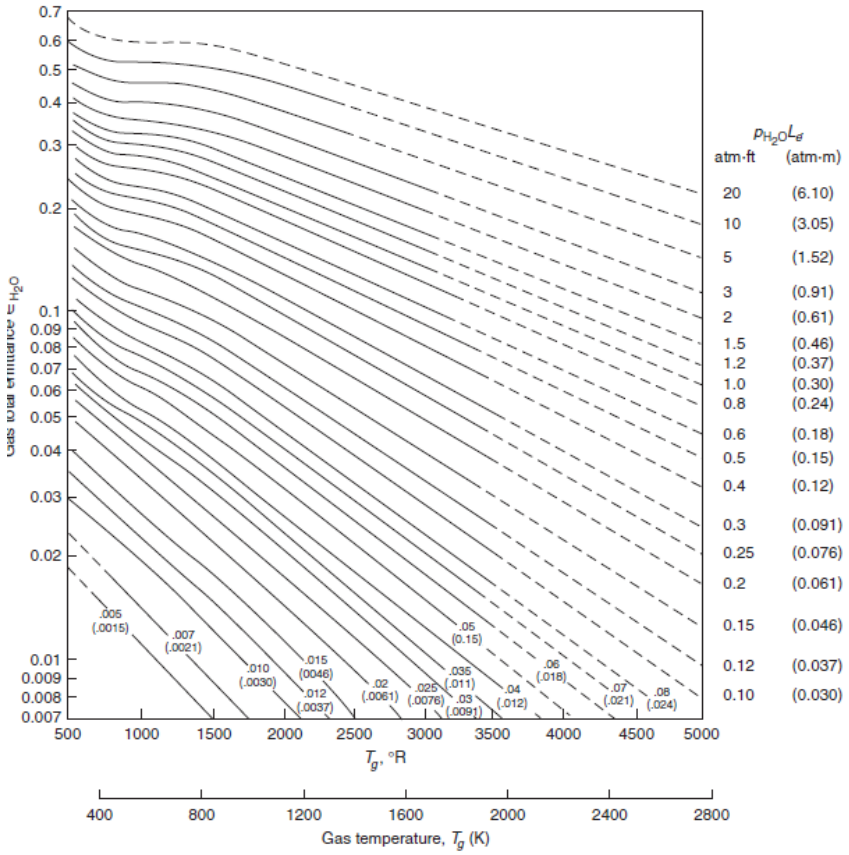

Figure 9:Total emissivity of water-vapor in a mixture of total pressure of 1 atm [8]

Wind Driven Convection Heat Transfer and Surface Level Analysis

Calculating the wind driven forced convection and the resultant contribution to the heat transfer of the surface of the adjacent ESS is subject to numerous assumptions. For the purposes of establishing bounding conditions where heat transfer is bounded and follows the work of Cengel [70].

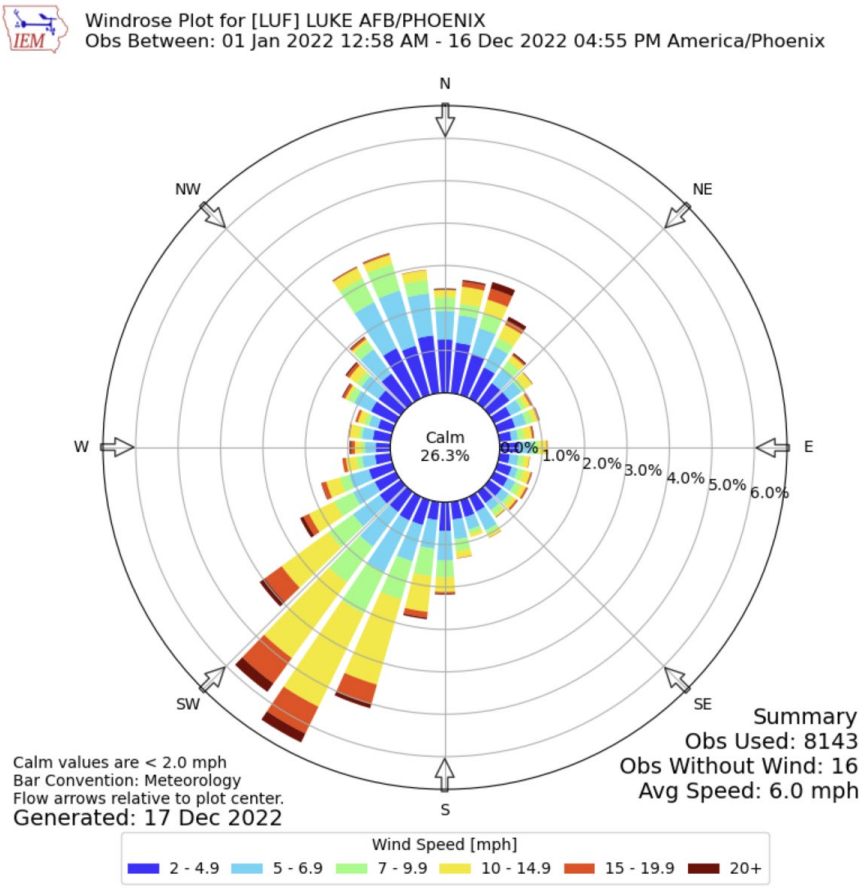

Figure 10: Luke AFB Windrose Data Example

It is assumed a 4.16m/s wind event over the top of an engaged ESS will follow the principles in the transition from laminar to turbulent flow depends on the surface geometry, flow velocity, surface temperature, and type of fluid. For the purposes of this analysis, surface roughness is assumed to be negligible.

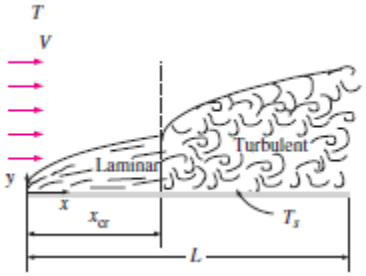

Figure 11:Analyzed Forced Convection over the top of the Engaged ESS

Assuming the top of the ESS to be a flat plate for maximum heat transfer, the Reynolds Number, the transition point where the air flow transitions from laminar to turbulent over a flat plate is governed by

$$Re_L = \frac{L\,V_L}{\nu}$$

Where L is the length of the headed surface (2.232 m, top of ESS)
V_L is the velocity of the wind event (4.165m/s)
ν is the kenetic viscosity of air (1.338×10^{-5} m/s at 20°C) [71]

Given the Reynolds number is less than the ideal (5×10^5), it is determined there is both turbulent and

laminar flow over the ESS. Given the thermal conductivity of air (k = 0.02514) and the Prandt number (P_r, 0.977 at 20°C for Sun City AZ), the Nusselt Number (Nu) numbers for laminar assuming uniform heat flux from the surface of the ESS is

$$Nu_L = (0.664\, Re_x^{0.8}) Pr^{\frac{1}{3}}$$

The net heat flux from the top of the container assuming a heat transfer coefficient of 62.5 kW/hr ($h = {}^{k}/_{L}\, Nu$) and applying the classical forced convection heat transfer equation [70] below

$$Q_{conv} = h\, A_s (T_1 - T_2)$$

and given the naturally occurring upward lift and wall shear of the heated air, assuming a bounding condition where 50% of the heat transfer due to convection is pulled into the wake region between ESSs, the total heat flux to the surface of the adjacent ESS is

$$q'_{Total} = q'_{Con} + q'_{Rad}$$

The wind driven surface temperature of the adjacent ESS due to normal heat propagation, wind velocity, and direction will have an additional intermittent contribution of 365 kW/m^2 to the first responders approximately 6.5' away as shown in Figure 13.

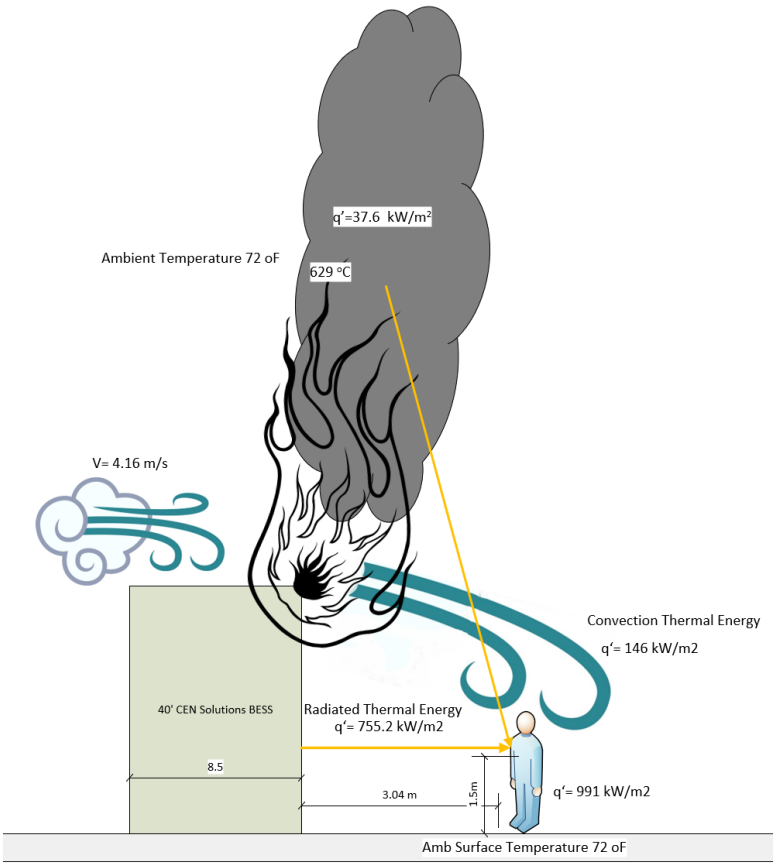

Figure 12: Maximum Theoretical Radiated Heat Flux at 10' (3.04m)

Table 2: Theoretical Momentary Heat Flux as a Function of Distance

Distance	Momentary Maximum Theoretical Heat Flux (kW/m^2)
10’	939
20’	589
30’	348
40’	235
50’	170
60’	127
70’	98
80’	77
90’	62
100’	51

Internal Temperature of Adjacent Target ESS

The rate of heat conduction through the adjacent container wall and internal container surface temperature would be determined by manipulation of [51]

$$\dot{q}''_{rec.adj.ESS} = A\sqrt{\frac{\pi}{4}\frac{k\rho c}{t}}\left(T_{adj.ESS.surface} - T_{adj.ss.int}\right)$$

Assuming the application of a typical Polyurethane insulation product with a Thermal Conductance of 0.22, the temperature on the internal surface is determined through manipulation of

$$\dot{q}''_{rec.adj.ESS} = \frac{k}{L}\left(T_{adj.ss.int} - T_{adj.int}\right)$$

Polyurethane performance above 130 °C is not published, therefore the Thermal Conductance is assumed to be degraded to approximately 0.05.

Considering the geometric focus factors of a CEN 40’ CEN across an 6.5’ passageway, the atmospheric attenuation factors, assuming black-body radiated heat emanating from the painted iron fully engage BESS to an adjacent ESS, and radiation and convection heat transfer from the EnerC and the released fire plume could reach a momentary 1148 kW/m^2. The calculated steady-state interior temperature of the CEN 40’ BESS across the 6.5’ passageway may experience approximately a 420K (147 °C) increase. Once the internal thermal management is no longer in operation, the heat transfer from the adjacent fully developed container fire could, as a function of the fire lifecycle and thermal insulation degradation, likely exceed the thermal stability thresholds of the adjacent BESS requiring additional mitigation strategies (i.e., use of fire water for evaporative cooling).

Theoretical Toxic Composition of Smoke Plume

It is well documented that Lithium-ion battery fires generate intense heat and considerable amounts of gas and smoke [21, 34, 55, 61, 72-78]. Although the emission of toxic gases can be a larger threat than the heat, the knowledge of such emissions is limited for large grid-connected energy storage systems. Therefore, the following discussion outlines the findings of research into peer-reviewed publications and government sources to identify the potential toxic gas constituents in a ESS fire.

New York State Energy Research & Development Authority (NYSERDA) and Consolidated Edison, the New York City Fire Department (FDNY) and the New York City Department of Buildings (NY DOB), DNV-GL was commissioned to address code and training updates required to accommodate deployment of energy storage in New York City. The research by NYSERDA concluded "that all batteries tested emitted toxic fumes, the toxicity is similar to a plastics fire and therefore a precedent exists"[55]. Several different manufacturer battery cells were tested and the typical gases emitted included:

- Carbon monoxide (CO)
- Hydrochloride (HCl)
- Hydrogen Fluoride (HF)
- Hydrogen Cyanide (HCN)

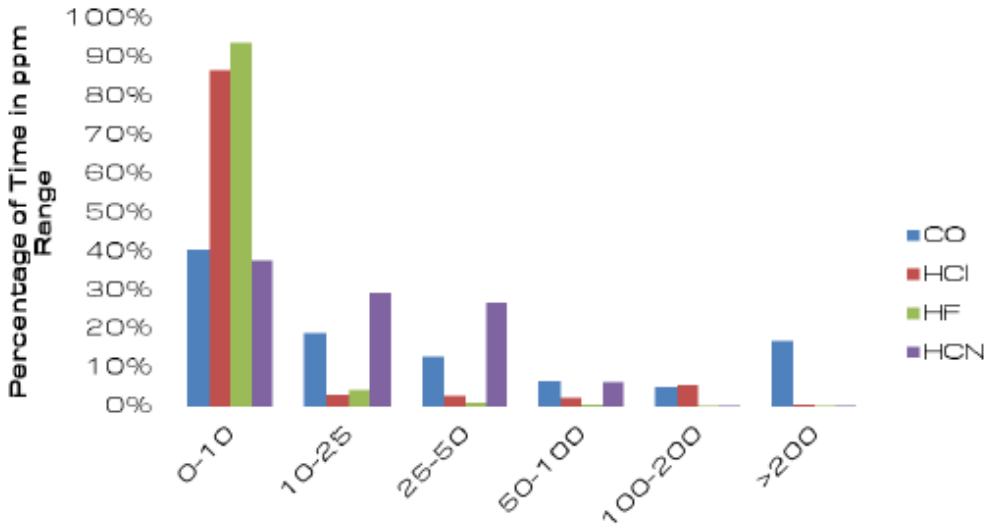

Figure 13: Representative emissions histogram from a Li-ion battery

DNV-GL concluded the "average emissions rate of a battery during a fire condition is lower per kilogram of material than a plastics fire"…."However, the peak emissions rate (during thermal runaway of a Li-ion battery, for example) is higher per kilogram of material than a plastics fire. This illustrates that a smoldering Li-ion battery on a per kilogram basis can be treated with the same precautions as something like a sofa, mattress, or office fire in terms of toxicity, but during the most intense moments of the fire (during the 2-3 minutes that cells are igniting exothermically) precautions for toxicity and ventilation should be taken. It should be noted that if Li-ion battery modules are equipped with cascading protections, the cell failure rate may be randomized and staggered. The randomized failure rate limits the toxicity and heat release rate of the fire"[55]. However, few studies have been published that report measurements of released HF amounts from commercial Li-ion battery cells during abuse and HF release during electrolyte fire tests [59, 61, 75].

Larsson et al. studied a broad range of commercial Li-ion battery cells with different chemistry, cell design and size and included large-sized automotive-classed cells, undergoing fire tests. Their objective was to evaluate fluoride gas emissions for a large variety of battery types and for various test setups. Based on their specialized results, they determined as a function of LIB design, a wide range of amounts of HF, ranging between 20 and 200 mg/Wh of nominal battery energy capacity, were detected from the burning Li-ion batteries [37, 59, 75].

Larsson determined the vented gases can contain evaporated solvents and decomposition products, e.g. CO, CO2, H2, CH4. Beside CO, a large number of different toxic compounds can be released including fluoride gases and most concerningly Hydrogen fluoride (HF). The fluorine in the cells comes from the Li-salt, e.g. LiPF6, but also from electrode binders, e.g. PVdF, electrode materials and coatings, e.g. fluorophosphates and AlF3-coated cathodes, as well as from fluorine containing additives, e.g. flame retardants [59]. PF_5, POF_3 and HF are of greatest concern but consideration should also be given to the fluorinated phosphoric acids since they will give HF and phosphoric acid when completely reacted with water [61].

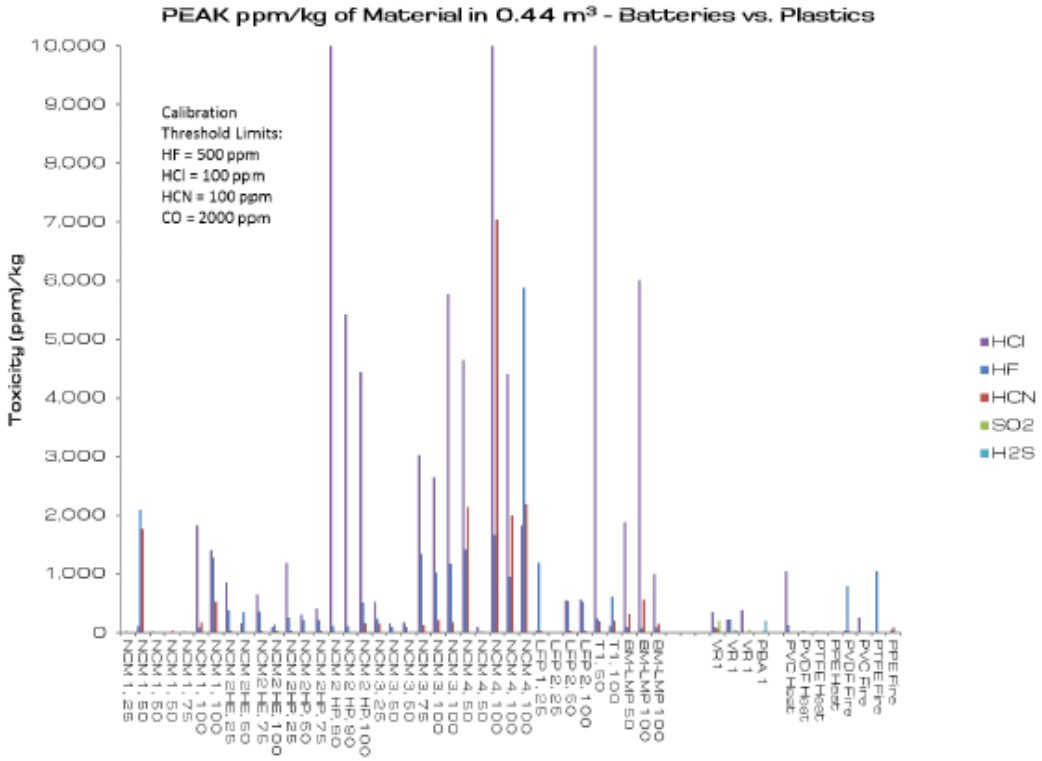

Figure 14: Peak ppm per kg (in a 0.44 m3 volume) for all batteries tested as compared to plastics [55]

The National Institute for Occupational Safety and Health (NIOSH) states that HF has a Immediately Dangerous to Life and health (IDLH) value of 30 ppm as shown in Table 3 [79]. No exposure limits are given for Phosphorus pentafluoride (PF_5) and Phosphoryl fluoride (POF_3), however their chlorine analogues, Phosphorus pentachloride (PCl_5) and Phosphoryl chloride ($POCl_3$) have recommended exposure limits (REL) values of 0.1 ppm [79].

As it pertains to the Samsung SDI NMC cells, the work performed by the SP Technical Research Institute of Sweden when testing NMC, lithium ion phosphate cells, determined the measured concentrations of HF were "generally quite low but well above the detection limits" [61].

The SP Technical Research Institute of Sweden concluded based on their research "POF_3 was detected in all the small scale tests using pure electrolyte. However, no POF_3 was detected in the tests on cells. The detection limit for POF_3 was 6 ppm. Extrapolating from the small scale tests to the cells tests one ends up at concentrations below 6 ppm, which probably explains why no POF_3 was detected in these tests" [61]. "It is an important finding that POF_3 is emitted from a battery fire as this will increase the toxicity of the fire effluents. The amount of POF_3 is shown to be significant, 5-40 % of the HF emissions on a weight basis.

No PF5 could be detected in any of the tests" [61].

Table 3: NIOSH Chemical Listing for Hydrogen Fluoride (HF)

Hydrogen fluoride	**Formula:** HF	**CAS#:** 7664-39-3	**RTECS#:** MW7875000	**IDLH:** 30 ppm
Conversion: 1 ppm = 0.82 mg/m^3	**DOT:** 1052 125 (anhydrous); 1790 157 (solution)			
Synonyms/Trade Names: Anhydrous hydrogen fluoride; Aqueous hydrogen fluoride (i.e., Hydrofluoric acid); HF-A				
Exposure Limits: **NIOSH REL:** TWA 3 ppm (2.5 mg/m^3) C 6 ppm (5 mg/m^3) [15-minute] **OSHA PEL†:** TWA 3 ppm **Physical Description:** Colorless gas or fuming liquid (below 67°F) with a strong, irritating odor. [**Note:** Shipped in cylinders.]			**Measurement Methods (see Table 1):** **NIOSH** 3800, 7902, 7903, 7906 **OSHA** ID110	
Chemical & Physical Properties: **MW:** 20.0 **BP:** 67°F **Sol:** Miscible **FI.P:** NA **IP:** 15.98 eV **RGasD:** 0.69 **Sp.Gr:** 1.00 (Liquid at 67°F) **VP:** 783 mmHg **FRZ:** -118°F **UEL:** NA **LEL:** NA Nonflammable Gas	**Personal Protection/Sanitation (see Table 2):** **Skin:** Prevent skin contact (liquid) **Eyes:** Prevent eye contact (liquid) **Wash skin:** When contam (liquid) **Remove:** When wet or contam (liquid) **Change:** N.R. **Provide:** Eyewash (liquid) Quick drench (liquid)		**Respirator Recommendations (see Tables 3 and 4):** **NIOSH/OSHA** **30 ppm:** CcrS*/PaprS*/GmFS/Sa*/ScbaF **§:** ScbaF:Pd,Pp/SaF:Pd,Pp:AScba **Escape:** GmFS/ScbaE	
	Incompatibilities and Reactivities: Metals, water or steam [**Note:** Corrosive to metals. Will attack glass and concrete.]			
Exposure Routes, Symptoms, Target Organs (see Table 5): **ER:** Inh, Abs (liquid), Ing (solution), Con **SY:** Irrit eyes, skin, nose, throat; pulm edema; eye, skin burns; rhinitis; bron; bone changes **TO:** Eyes, skin, resp sys, bones		**First Aid (see Table 6):** **Eye:** Irr immed (solution/liquid) **Skin:** Water flush immed (solution/liquid) **Breath:** Resp support **Swallow:** Medical attention immed (solution)		

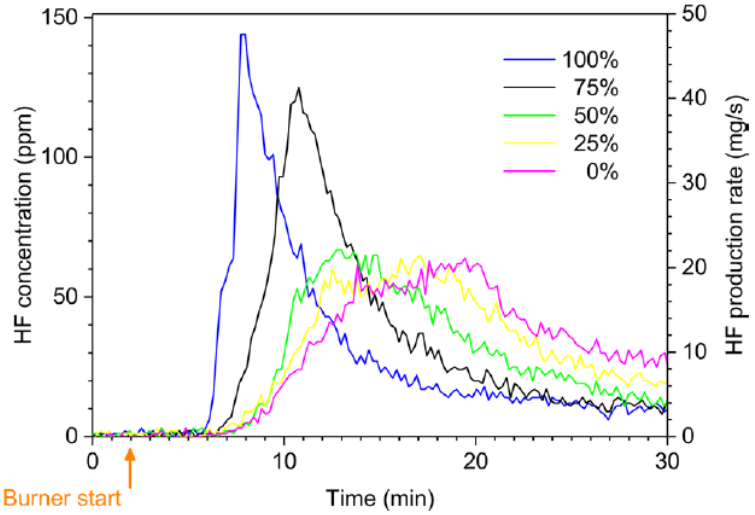

Figure 15: HF release both as the measured concentrations[75]

Lithium Ion ESS Fire Smoke Plume Research Conclusion

Research has shown the complex mixture of flammable and toxic gases are emitted from the thermal decomposition of LIB is manufacturer and chemistry dependent. The composite breakdown of particles is a function of the size of the energy source and the inherent design chemistry that can only be estimated based on the research of others. To date, there is no readily identifiable performance data for the Samsung E4L batteries used in the Samsung SDI applications. Therefore, the following list of potentially flammable and toxic gases is theoretical based on the cited works of [21, 34, 55, 61, 72-78]:

Table 4: List of Potential Emitted Gases during Thermal Runaway.

Gases Measured	Chemical Formula	Gas Type
Acetylene	C2H2	Hydrocarbons
Ethylene	C2H4	Hydrocarbons
Ethane	C2H6	Hydrocarbons
Methane	CH4	Hydrocarbons
Methanol	CH3OH	Hydrocarbons
Formaldehyde	CH2O	Hydrocarbons (Aldehydes)
Hydrogen Bromide	HBr	Hydrogen Halides
Hydrogen Chloride	HCl	Hydrogen Halides
Hydrogen Fluoride	HF	Hydrogen Halides
Hydrogen Sulfide	H2S	Sulfur Containing
Carbon Dioxide	CO2	Carbon Containing
Carbon Monoxide	CO	Carbon Containing
Ammonia	NH3	Nitrogen Containing
Hydrogen Cyanide	HCN	Nitrogen Containing
Hydrogen	H2	-
Sulfur Dioxide	SO2	Sulfur Containing

It is noted, that while the DNV-GL/NYSERDA report lists only 4 emitted gases, CSA testing of the Samsung

SDI 112 Ah batteries measured the following emitted gases:

- "Carbon dioxide (CO2)
- Carbon monoxide (CO)
- Methane (CH4)
- Ethylene (C2H4)
- Ethane (C2H6)
- Propene (C3H6)
- Propane (C3H8)
- Hydrogen (H2)"[80]

Recommended Minimum Approach Distance

The Occupational Safety and Health Administration requires employers to establish minimum approach distance (MAD) as "the closest distance a qualified employee may approach an energized conductor or object" [81]. While directly applicable to energized circuits, the requirement of notifying employees of occupational hazards and risks and establishing both engineering and administrative controls is presented in 29CFR 1910. For the purposes of this analysis, the Minimum Approach Distance is defined as the closet distance a qualified employee may approach a known hazard.

While there are several different organizations (ACGIH, AIHA, OSHA, ISO, and NIOSH) that establish controls for hazard exposure, all require a job hazard analysis (JHA) be conducted to identify the hazard controls. It is assumed the appropriate JHA will be performed for each scheduled task when operating and maintaining the Samsung SDI energy storage systems.

Table 2 presents the radiated heat flux as a function of distance from a fully engaged energy storage system. Table 5 presents the physiological effects of thermal radiation and the time of exposure to extreme pain and 2nd degree burns.

Table 5: Physiological Effects of Thermal Radiation [82]

Time for Physiological Effects (on bare skin) to Occur Following Exposure to Specific Thermal Radiation Levels		
Radiation Intensity (kW/m2)	Time for Severe Pain (seconds)	Time for 2nd Degree Burn (seconds)
1	115	663
2	45	187
3	27	92
4	18	57
5	13	40
6	11	30
8	7	20
10	5	14
12	4	11

Therefore, it is recommended the Minimum Approach Distances for First Responders be set at a

conservative distance of 50 ft. when responding to a fire due to the potential radiated heat and HF exposure.

Scenarios

From a fire protection standpoint, the overall fire hazard of any ESS is a combination of all the combustible system components, including battery chemistry, battery format (e.g., cylindrical, prismatic, polymer pouch), battery capacity and energy density, materials of construction, and component design (e.g., battery, module). To ensure confidence in the conservative approach for this FRA, the ESS are assumed to be operating under a normal operating condition, such that proprietary electronic protection systems, e.g., battery management system (BMS), are active. It is recognized any benefit from these proprietary systems would further reduce the overall hazard, e.g., the likelihood of ignition, but is not necessary to ensure the adequacy of the protection.

The enabling assumption of the fire scenario is based on the numerous published energy storage system fires with a probability of occurrence of less than 1 % across the global ESS market sector. Based on the UL9540A Cell, Module, and Unit Level Testing, and understanding the lack of propagation when heated to thermal runaway temperatures, the likelihood of a sustained fire within the Samsung SDI is reasonably less than 1%.

Data Sources

[1] D. Hill, "Technical Support for APS Related to Mcmicken Thermal Runaway and Explosion: McMicken Battery Energy Storage System Event Technical Analysis and Recommendations," DNV GL Energy Insights USA, Inc., Chalfont, PA, 18 July 2020 2020.

[2] UL, "Unit Test Report - UL 9540A Test Method for Evaluating Thermal Runaway Fire Propagation in Battery Energy Storage Systems (AACD)," Underwriters Laboratory, Northbrook IL, 20 January 2022.

[3] UL, "Module Test Report - UL 9540A Test Method for Evaluating Thermal Runaway Fire Propagation in Battery Energy Storage Systems (AACD)," Underwriters Laboratory, Northbrook IL, 20 January 2022.

[4] UL, "Cell Test Report - UL 9540A Test Method for Evaluating Thermal Runaway Fire Propagation in Battery Energy Storage Systems (AACD)," Underwriters Laboratory, Northbrook IL, 14 October 2020.

[5] UL, "Installation Test Report - UL 9540A Test Method for Evaluating Thermal Runaway Fire Propagation in Battery Energy Storage Systems (AACD)," Underwriters Laboratory, Northbrook IL, 17 May 2022.

[6] NFPA, "NFPA 551: guide for the evaluation of fire risk assessments," *National Fire Protection Association, Quincy, USA,* 2016.

[7] *Engineering Guide: Fire Risk Assessment*, SFPE, Gaithersburg, MD, 2006.

[8] M. J. Hurley *et al.*, *SFPE Handbook of Fire Protection Engineering*. Quincy, Massachusetts: National Fire Protection Association, 2015.

[9] *ISO 16732-1: Fire Safety Engineering - Fire RIsk Assessment, Part 1 - General*, ISO, Geneva, Switzerland, 15 February 2012 2012.

[10] *ISO 16732-1: Fire Safety Engineering - Fire RIsk Assessment, Part 3: Example of an Industrial Property*, ISO, Geneva, Switzerland, 15 February 2012 2012.

[11] DOE, "U.S. Battery Storage Market Trends," ed. Washington DC: US Department of Energy, US Energy Information Administration 2018.

[12] DNV-GL, "McMicken Battery Energy Storage System Event Technical Analysis and

Recommendations," Chalfont, PA, 18 July 2020 2020.

[13] D. Belov and M.-H. Yang, "Failure mechanism of Li-ion battery at overcharge conditions," *Journal of Solid State Electrochemistry,* vol. 12, no. 7-8, pp. 885-894, 2008. [Online]. Available: https://www.researchgate.net/profile/Dmitry_Belov6/publication/226507209_Failure_mechanism_of_Li-ion_battery_at_overcharge_conditions/links/56fb42cb08ae8239f6dadb98.pdf.

[14] N. Ponchaut, K. Marr, F. Colella, V. Somandepalli, and Q. Horn, "Thermal runaway and safety of large lithium-ion battery systems," *Proceedings of the The Battcon,* pp. 17.1-17.10, 2015.

[15] F. Xu *et al.*, "Failure investigation of LiFePO4 cells under overcharge conditions," *Journal of The Electrochemical Society,* vol. 159, no. 5, p. A678, 2012.

[16] Z. Wang, K. Zhu, J. Hu, and J. Wang, "Study on the fire risk associated with a failure of large-scale commercial LiFePO4/graphite and LiNixCoyMn1-x-yO2/graphite batteries," *Energy Science & Engineering,* vol. 7, no. 2, pp. 411-419, 2019.

[17] S. Wang, Z. Du, Z. Han, Z. Zhang, L. Liu, and J. Hao, "Study of the Temperature and Flame Characteristics of Two Capacity LiFePO4 Batteries in Thermal Runaway," *Journal of The Electrochemical Society,* vol. 165, no. 16, pp. A3828-A3836, 2018, doi: 10.1149/2.0531816jes.

[18] Q. Wang, P. Ping, X. Zhao, G. Chu, J. Sun, and C. Chen, "Thermal runaway caused fire and explosion of lithium ion battery," *Journal of power sources,* vol. 208, pp. 210-224, 2012.

[19] Q. Wang, B. Mao, S. I. Stoliarov, and J. Sun, "A review of lithium ion battery failure mechanisms and fire prevention strategies," *Progress in Energy and Combustion Science,* vol. 73, pp. 95-131, 2019.

[20] P. Ping *et al.*, "Study of the fire behavior of high-energy lithium-ion batteries with full-scale burning test," *Journal of Power Sources,* vol. 285, pp. 80-89, 2015.

[21] D. Ouyang, M. Chen, Q. Huang, J. Weng, Z. Wang, and J. Wang, "A review on the thermal hazards of the lithium-ion battery and the corresponding countermeasures," *Applied Sciences,* vol. 9, no. 12, p. 2483, 2019.

[22] X. Li and Z. Wang, "A novel fault diagnosis method for lithium-Ion battery packs of electric vehicles," *Measurement,* vol. 116, pp. 402-411, 2018.

[23] B. Ditch and D. Zeng, "Research Technical Report: Development of Sprinkler Protection Guidance for Lithium Ion Based Energy Storage Systems," FM Global, Norwood, MA, June 2019 2019.

[24] NFPA, "Sprinkler Protection Guidance for Lithium-Ion Based Energy Storage Systems," National Fire Protection Association, Quincy, MA USA, June 2019 2019. [Online]. Available: https://www.nfpa.org//-/media/Files/News-and-Research/Fire-statistics-and-reports/Suppression/RFESSSprinklerProtection.pdf

[25] A. E. Cote, *NFPA No.: FPH2008 - Fire Protection Handbook*, Twentieth Edition ed. Quincy, MA: National Fire Protection Assoc, 2008.

[26] CSA, "Project 80040846: CSA Group hereby confirms that it has completed an evaluation of: Li-ion Battery Cell, models 001CB310, CB310 and CB2W0," CSA Group, Ningde City, China, Project 80040846, 22 July 2020.

[27] S. Koch, K. Birke, and R. Kuhn, "Fast thermal runaway detection for lithium-ion cells in large scale traction batteries," *Batteries,* vol. 4, no. 2, p. 16, 27 March 2018 2018. [Online]. Available: www.mdpi.com/journal/batteries.

[28] M. Ghiji *et al.*, "A Review of Lithium-Ion Battery Fire Suppression," *Energies,* vol. 13, no. 19, p. 5117, 2020.

[29] R. T. L. Jr., J. A. Sutula, and M. J. Kahn, "Lithium Ion Batteries Hazard and Use Assessment

Phase IIB, Flammability Characterization of Li-ion Batteries for Storage Protection," The Fire Protection Research Foundation, Quincy MA, April 29, 2013 2013.

[30] L. Kong, C. Li, J. Jiang, and M. Pecht, "Li-ion battery fire hazards and safety strategies," *Energies,* vol. 11, no. 9, p. 2191, 2018.

[31] S. Cummings. "South Korea Identifies Top 4 Causes that Led to ESS Fires." Li-ion Tamer. https://liiontamer.com/south-korea-identifies-top-4-causes-that-led-to-ess-fires/ (accessed 26 July 2019, 2019).

[32] S. J. Harris, D. J. Harris, and C. Li, "Failure statistics for commercial lithium ion batteries: A study of 24 pouch cells," *Journal of Power Sources,* vol. 342, pp. 589-597, 2017.

[33] J. Lamb, C. J. Orendorff, L. A. M. Steele, and S. W. Spangler, "Failure propagation in multi-cell lithium ion batteries," *Journal of Power Sources,* vol. 283, pp. 517-523, 2015.

[34] J. Lamb, C. J. Orendorff, E. P. Roth, and J. Langendorf, "Studies on the thermal breakdown of common Li-ion battery electrolyte components," *Journal of The Electrochemical Society,* vol. 162, no. 10, pp. A2131-A2135, 2015.

[35] W. Tang, W. C. Tam, L. Yuan, T. Dubaniewicz, R. Thomas, and J. Soles, "Estimation of the critical external heat leading to the failure of lithium-ion batteries," *Applied thermal engineering,* vol. 179, p. 115665, 2020.

[36] A. Sarkar, I. C. Nlebedim, and P. Shrotriya, "Performance degradation due to anodic failure mechanisms in lithium-ion batteries," *Journal of Power Sources,* vol. 502, p. 229145, 2021.

[37] F. Larsson, P. Andersson, P. Blomqvist, A. Lorén, and B.-E. Mellander, "Characteristics of lithium-ion batteries during fire tests," *Journal of Power Sources,* vol. 271, pp. 414-420, 2014.

[38] F. Larsson, P. Andersson, P. Blomqvist, and B.-E. Mellander, "Toxic fluoride gas emissions from lithium-ion battery fires," *Scientific reports,* vol. 7, no. 1, pp. 1-13, 2017.

[39] N. Williard, W. He, C. Hendricks, and M. Pecht, "Lessons learned from the 787 Dreamliner issue on lithium-ion battery reliability," *Energies,* vol. 6, no. 9, pp. 4682-4695, 2013.

[40] J. Vetter *et al.*, "Ageing mechanisms in lithium-ion batteries," *Journal of power sources,* vol. 147, no. 1-2, pp. 269-281, 2005.

[41] *UL 1642 UL Standard for Safety Lithium Batteries*, UL, Nrothbrook, IL, 29 September 2020 2020.

[42] Celina Mikolajczak, Michael Kahn, Kevin White, and Richard Thomas Long, "Lithium-Ion Batteries Hazard and Use Assessment - Final Report," The Fire Protection Research Foundation, Quincy MA, July 2011 2011.

[43] "IEEE Standard for Rechargeable Batteries for Multi-Cell Mobile Computing Devices," *IEEE Std 1625-2008 (Revision of IEEE Std 1625-2004),* pp. c1-79, 2008, doi: 10.1109/IEEESTD.2008.4657368.

[44] *ANSI/CAN/UL-1973:2018, Batteries for Use in Stationary, Vehicle Auxiliary Power and Light Electric Rail (LER) Applications*, UL, Northbrook, IL, February 7, 2018 2018.

[45] UL, "Module Test Report UL 9540A Test Method for Evaluating Thermal Runaway Fire Propagation in Battery Energy Storage Systems (AACD) [Samsung SDI MS8943E101A]," Underwriters Laboratory, GYEONGGI-DO, Republic of Korea, 4789768841, 25 May 2022.

[46] NHTSA, "Lithium-ion Battery Safety Issues for Electric and Plug-in Hybrid Vehicles," US Department of Transportation, National Highway Traffic Safety Administration, Washington D.C., October 2017 2017. [Online]. Available: https://www.nhtsa.gov/sites/nhtsa.dot.gov/files/documents/12848-lithiumionsafetyhybrids_101217-v3-tag.pdf

[47] A. Blum and R. Long Jr, "Lithiu m Ion Batteries Hazard and Use Assessment - Phase III," in "Fire Protection Research Foundation," Fire Protection Research Foundation, Quincy, MA,

November 2016 2016.

[48] A. F. Blum and R. T. Long Jr, *Fire Hazard Assessment of Lithium Ion Battery Energy Storage Systems*. Springer Nature, 2016.

[49] DNV-GL, "Safety, Operation and Performance of Grid Connected Energy Storage Systems," vol. DNVGL-RP-0043, ed. Oslo, Norway: Det Norske Veritas Holding AS, 2017.

[50] UL, "Cell Test Report: UL 9540A Test Method for Evaluating Thermal Runaway Fire Propagation in Battery Energy Storage Systems (AACD)," Underwriters Laboratory, LLC, Fujian, CN, 27 December 2019.

[51] J. Quintiere, *Fundamentals of fire phenomena*. Wiley, 2006.

[52] M. Greenwood, M. Wentker, and J. Leker, "A bottom-up performance and cost assessment of lithium-ion battery pouch cells utilizing nickel-rich cathode active materials and silicon-graphite composite anodes," *Journal of Power Sources Advances,* vol. 9, p. 100055, 2021.

[53] G. Mulder *et al.*, "Comparison of commercial battery cells in relation to material properties," *Electrochimica Acta,* vol. 87, pp. 473-488, 2013.

[54] T. Ohsaki *et al.*, "Overcharge reaction of lithium-ion batteries," *Journal of Power Sources,* vol. 146, no. 1-2, pp. 97-100, 2005.

[55] DNV-GL, "Considerations for ESS Fire Safety," 3rd ed. Dublin, OH: Det Norske Veritas (U.S.A.), Inc. (DNV GL), 2017.

[56] C. Edison, "Considerations for ESS Fire Safety," DET NORSKE VERITAS (U.S.A.),, Dublin, OH, OAPUS301WIKO(PP151894), Rev. 3, January 18th, 2017 2017. [Online]. Available: https://nysolarmap.com/media/1718/dg-hubbess-con-edison-nyserda-final-report-11817.pdf

[57] UL, "UL 9540A Test Method for Evaluating Thermal Runaway Fire Propagation in Battery Energy Storage Systems: Module Level Test Report - Model EM048290P5B1," UL Research and Development, Energy & Power Technologies, Washington D.C., 2019.

[58] UL, "UL 9540a Test Method for Evaluating Thermal Runaway Fire Propagation in Battery Energy Storage Systems," UL Research and Development, Energy & Power Technologies, Washington D.C., 2018-06-15 2018.

[59] F. Larsson, S. Bertilsson, M. Furlani, I. Albinsson, and B.-E. Mellander, "Gas explosions and thermal runaways during external heating abuse of commercial lithium-ion graphite-LiCoO2 cells at different levels of ageing," *Journal of power sources,* vol. 373, pp. 220-231, 2018.

[60] F. Larsson and B.-E. Mellander, "Abuse by external heating, overcharge and short circuiting of commercial lithium-ion battery cells," *Journal of The Electrochemical Society,* vol. 161, no. 10, p. A1611, 2014.

[61] P. Andersson, P. Blomqvist, A. Loren, and F. Larsson, *Investigation of fire emissions from Li-ion batteries*. 2013.

[62] M. Held *et al.*, "Thermal runaway and fire of electric vehicle lithium-ion battery and contamination of infrastructure facility," *Renewable and Sustainable Energy Reviews,* vol. 165, p. 112474, 2022.

[63] Z. Wang, H. Yang, Y. Li, G. Wang, and J. Wang, "Thermal runaway and fire behaviors of large-scale lithium ion batteries with different heating methods," *Journal of hazardous materials,* vol. 379, p. 120730, 2019.

[64] X. Tian *et al.*, "Design strategies of safe electrolytes for preventing thermal runaway in lithium ion batteries," *Chemistry of Materials,* vol. 32, no. 23, pp. 9821-9848, 2020.

[65] A. Blum and R. Long Jr, "Hazard assessment of lithium ion battery energy storage systems," in "Fire Protection Research Foundation," Fire Protection Research Foundation, Bowie, MD, February 2016 2016.

[66] D. Pitts and L. Sissom, *Schaum's Outline of Theory and Problems of Heat Transfer* 2ed.

(Schaum's Outline Series). New York, NY: McGraw Hill, 1988.
[67] C. Choy and D. Greig, "The low temperature thermal conductivity of isotropic and oriented polymers," *Journal of Physics C: Solid State Physics,* vol. 10, no. 2, p. 169, 1977.
[68] J. Pokorný, "Determination of centreline temperature of Fire Plume with respect to a gas hot layer," presented at the Fire Engineernig, 3nd International Scientific Conference, Technical university in Zvolen, Slovak republic, January 2010, 2010. [Online]. Available: https://www.researchgate.net/publication/269990367_Determination_of_centreline_temperature_of_Fire_Plume_with_respect_to_a_gas_hot_layer.
[69] Z. Xing, J. Mao, Y. Huang, J. Zhou, W. Mao, and F. Deng, "Scaled experimental study on maximum smoke temperature along corridors subject to room fires," *Sustainability,* vol. 7, no. 8, pp. 11190-11212, 2015.
[70] Y. Cengel, *Heat and mass transfer: fundamentals and applications*. McGraw-Hill Higher Education, 2014.
[71] "Viscosity of Air, Dynamic and Kinematic." Engineers Edge, LLC. https://www.engineersedge.com/physics/viscosity_of_air_dynamic_and_kinematic_14483.htm (accessed 17 February 2020.
[72] A. Nedjalkov *et al.*, "Toxic gas emissions from damaged lithium ion batteries—analysis and safety enhancement solution," *Batteries,* vol. 2, no. 1, p. 5, 2016.
[73] DNV-GL, "Testing of Aerosol Fire Extinguishing Agent for Li-ion Battery Fires," vol. 10030271 – HOU – R -01, ed. Rochester, NY: Det Norske Veritas (DNV) GL - Energy Advisory Americas, 2017.
[74] UL, "UL 9540A Test Method for Evaluating Thermal Runaway Fire Propagation in Battery Energy Storage Systems Cell Level Test Report Model Model 6LH3L8," Underwriters Laboratory, Washington DC, Project Number 4788679452, 31 May 2019 2019.
[75] F. Larsson, P. Andersson, P. Blomqvist, and B.-E. Mellander, "Toxic fluoride gas emissions from lithium-ion battery fires," *Scientific reports,* vol. 7, no. 1, p. 10018, 2017.
[76] P. Ribière, S. Grugeon, M. Morcrette, S. Boyanov, S. Laruelle, and G. Marlair, "Investigation on the fire-induced hazards of Li-ion battery cells by fire calorimetry," *Energy & Environmental Science,* vol. 5, no. 1, pp. 5271-5280, 2012.
[77] A. Lecocq, G. G. Eshetu, S. Grugeon, N. Martin, S. Laruelle, and G. Marlair, "Scenario-based prediction of Li-ion batteries fire-induced toxicity," *Journal of Power Sources,* vol. 316, pp. 197-206, 2016.
[78] N. S. Spinner *et al.*, "Physical and chemical analysis of lithium-ion battery cell-to-cell failure events inside custom fire chamber," *Journal of Power Sources,* vol. 279, pp. 713-721, 2015.
[79] M. E. Barsan, "NIOSH pocket guide to chemical hazards," 2007.
[80] CSA, "UL 9540A - Test Method for Evaluating Thermal Runaway Fire Propagation in Battery Energy Storage Systems, 3rd edition for Li-ion Battery Cell, models 001CB310, CB310 and CB2W0, nominal voltage 3.2V, 280Ah," CCIC-CSA International Certification Co., Ltd. Kunshan Branch, Kunshan, China, 22 July 2020.
[81] (2021). *1926.968 - Definitions*. [Online] Available: https://www.osha.gov/laws-regs/regulations/standardnumber/1926/1926.968
[82] F. E. M. Agency, "Handbook of Chemical Hazard Analysis Procedures," ed: US EPAU. S. DOT, 1993.